SAPIENZA
UNIVERSITA' DI ROMA

DOTTORATO DI RICERCA IN MEDICINA SPERIMENTALE
XXX CICLO

Radiological evaluation of biomarkers for renal cell carcinoma

DOTTORANDO

Chiara Marigliano

DOCENTE GUIDA

Prof. Andrea Laghi

COORDINATORE DEL DOTTORATO
Prof.ssa Maria Rosaria Torrisi

ANNO ACCADEMICO 2016-2017

INDEX

1 – Introduction

Renal Cell Carcinoma

Renal cell carcinoma (RCC) is a heterogeneous disease accounting for about 90% of all renal malignancies and 1% to 3% of all malignant visceral neoplasms. Over the past few decades there has been a significant rise in incidence, likely explained with the recent advances in imaging technology in the diagnosis of localized cancer and the increase use of imaging in medical practice [1,2].

RCC includes multiple subtypes that differ in their histopathologic features, genetic expression pattern, and clinical behaviour.

During the last 2 decades, significant advances in the diagnosis, staging, and treatment of patients with RCC have resulted in improved survival in selected patients [3].

Recent discoveries in the genetics of RCC have provided the opportunity for new molecularly targeted therapies in patients with metastatic RCC, including immunotherapy and antiangiogenic therapies [4,5] The success of such targeted therapies relies on an accurate histologic subtyping of the tumours. Percutaneous biopsy can provide a pre-surgical ‘‘tissue diagnosis’’ in selected patients, although inaccurate tumour subtyping rates can be as high as 26% in sampled primary renal tumours [6,7]. Therefore, a method to accurately characterize the histology subtype of renal masses that is robust, non-invasive, and insensitive to sampling errors would have utility in clinical practice.

Approximately 40% of patients with RCC die because of the disease progression, thus this tumour is the most lethal malignant urological tumour.

Currently, most RCCs are incidentally found at imaging investigations.

Here is shown Table 1 with classification of Renal tumour as assessed by WHO 2016 Classification [8].

WHO classification of tumours of the kidney

Renal cell tumours	
Clear cell renal cell carcinoma	8310/3
Multilocular cystic renal neoplasm of low malignant potential	8316/1*
Papillary renal cell carcinoma	8260/3
Hereditary leiomyomatosis and renal cell carcinoma–associated renal cell carcinoma	8311/3*
Chromophobe renal cell carcinoma	8317/3
Collecting duct carcinoma	8319/3
Renal medullary carcinoma	8510/3*
MiT family translocation renal cell carcinomas	8311/3*
Succinate dehydrogenase–deficient renal carcinoma	8311/3
Mucinous tubular and spindle cell carcinoma	8480/3*
Tubulocystic renal cell carcinoma	8316/3*
Acquired cystic disease–associated renal cell carcinoma	8316/3
Clear cell papillary renal cell carcinoma	8323/1
Renal cell carcinoma, unclassified	8312/3
Papillary adenoma	8260/0
Oncocytoma	8290/0
Metanephric tumours	
Metanephric adenoma	8325/0
Metanephric adenofibroma	9013/0
Metanephric stromal tumour	8935/1
Nephroblastic and cystic tumours occurring mainly in children	
Nephrogenic rests	
Nephroblastoma	8960/3
Cystic partially differentiated nephroblastoma	8959/1
Paediatric cystic nephroma	8959/0
Mesenchymal tumours	
Mesenchymal tumours occurring mainly in children	
Clear cell sarcoma	8964/3
Rhabdoid tumour	8963/3
Congenital mesoblastic nephroma	8960/1
Ossifying renal tumour of infancy	8967/0
Mesenchymal tumours occurring mainly in adults	
Leiomyosarcoma	8890/3
Angiosarcoma	9120/3
Rhabdomyosarcoma	8900/3
Osteosarcoma	9180/3
Synovial sarcoma	9040/3
Ewing sarcoma	9364/3
Angiomyolipoma	8860/0
Epithelioid angiomyolipoma	8860/1*
Leiomyoma	8890/0
Haemangioma	9120/0
Lymphangioma	9170/0
Haemangioblastoma	9161/1
Juxtaglomerular cell tumour	8361/0
Renomedullary interstitial cell tumour	8966/0
Schwannoma	9560/0
Solitary fibrous tumour	8815/1
Mixed epithelial and stromal tumour family	
Cystic nephroma	8959/0
Mixed epithelial and stromal tumour	8959/0
Neuroendocrine tumours	
Well-differentiated neuroendocrine tumour	8240/3
Large cell neuroendocrine carcinoma	8013/3
Small cell neuroendocrine carcinoma	8041/3
Phaeochromocytoma	8700/0
Miscellaneous tumours	
Renal haematopoietic neoplasms	
Germ cell tumours	
Metastatic tumours	

The morphology codes are from the International Classification of Diseases for Oncology (ICD-O) (917A). Behaviour is coded /0 for benign tumours; /1 for unspecified, borderline, or uncertain behaviour; /2 for carcinoma in situ and grade III intraepithelial neoplasia; and /3 for malignant tumours. The classification is modified from the previous WHO classification (756A), taking into account changes in our understanding of these lesions.
*New code approved by the IARC/WHO Committee for ICD-O.

Clear cell renal cell carcinoma is the most common variant, representing almost 75% of all RCCs [9,10]. Only 5% of ccRCC are associated with hereditary syndromes (von Hippel-Lindau disease, tuberous sclerosis), most of them (95%) are sporadic.

Clear cell RCC originates from the proximal convoluted tubules epithelium (renal cortex) and presents a predominantly expansile growth pattern. Macroscopically, it is a solid, yellowish lesion with variable degrees of internal necrosis, hemorrhage and cystic degeneration. These findings are most frequently observed in large-volume, fast-growing tumours. Tumour calcifications may also be found. Clear cells are so named because of their lipid- and glycogen-rich cytoplasmic content [11]. Frequently, these tumours also present cell with eosinophil granular cytoplasm.

Imaging findings reproduce such histopatological features: they present as hypervascularized and heterogeneous lesions due to necrosis, hemorrhage, cysts and calcifications. Necrosis is more common generally in > 4 cm lesions. The rate of occurrence and degree of necrosis have also been associated with high-grade tumour histology [12,13]. At computed tomography (CT), ccRCC usually present with intense contrast enhancement in the corticomedullary phase (120–140 HU) and typical washout in the nephrographic phase (90–100 HU).

At MRI, at T1-weighted images we can find signal intensity similar to the one of the renal cortex, and hypersignal at T2-weighted images. Up to 60% of ccRCC because of the presence of intracellular lipid content, presents signal loss at out-of-phase image when the chemical shift imaging technique is employed [14]. It should be observed that this is a nonspecific finding of ccRCC, since it may also be seen in angiomyolipoma without macroscopic fat and, more rarely, also in pRCC. ccRCC may also present a hypodense pseudocapsule in the corticomedullary phase at CT, and with hyposignal at MRI T1- and T2-weighted sequences.

Discontinuity of this pseudocapsule generally indicates a high-grade tumour. Quantitative analysis of the contrast uptake by tumours at multiphase examinations (cortico-medullary,

nephrographic and excretory phases) demonstrated that the percentages of signal alteration in the three phases after contrast injection in relation to the pre-contrast phase were significantly higher in ccRCC than in pRCC or in crRCC.

Treatment

There is a wide spectrum of drugs with a good activity in advanced or metastatic renal cell carcinoma [15]. There is agreement on recommending targeted agents as the standard of care in this disease. Physicians and patients may select sunitinib, bevacizumab in combination with interferon- alpha (IFN-α), pazopanib, or—in poor risk patients—temsirolimus. There are also a variety of therapies with proven efficacy on hand in the second-line setting: sorafenib, pazopanib, axitinib, and everolimus.

Currently, seven drug or drug combinations are licensed for the treatment of metastatic RCC. Crucial for this progress was the understanding of the role of angiogenesis in general and the VEGF- and mTOR-pathways [16].

The biggest problem in RCC is relapse, that’s why good guidelines for the correct sequence of agents is needed to achieve the best response, at least stabilizing the disease. The sequence for using these therapies is an ongoing matter of debate and several reviews have been published on this topic over the past years [17]

Here are shown tables from Fisher et All [18] which show treatment option at first, second and third line.

Table 1 First-line treatment

Risk group	Standard	Option
Good or intermediate	Sunitinib [I, A]	High-dose IL-2 [III, C]
	Pazopanib [I, A]	Bevacizumab + low-dose IFN-α [III, B]
	Bevacizumab + IFN-α [I, A]	
Poor	Temsirolimus [I, A]	Sunitinib [II, B]

IFN-α, interferon-alpha.

Table 2 Second-line treatment

Prior treatment	Standard	Option
TKI	Axitinb [I, B]	Sorafenib [II, B]
	Everolimus [II, B]	
Bev + IFN-α	Sunitinib [III, B]	

TKI, tyrosine kinase inhibitors; IFN-α, interferon-alpha.

Table 3 Third-line treatment

Prior treatment	Standard	Option
2 TKIs	Everolimus [II, B]	
TKI + mTOR inhibitor	Sorafenib [I, B]	Other TKI [IV, B]
		Re-challenge [IV, B]

TKI, tyrosine kinase inhibitors; mTOR, mammalian target of rapamycin.

Mechanisms of resistance to anti-angiogenetic therapy are multiple, one of these is up-regulation of alternative pro-angiogenic pathways [19]. Further studies showed up-regulation of pro-angiogenic factors such as PDGF and FGF [20] after angiogenesis inhibition. Other mechanism could be activation of mTOR-pathway which integrates information about nutrients and growth factors and has a central role in cell growth and cell cycle progression.

Microenviroment such as lower oxygen levels seem to lead to recruitment of vascular progenitor cells from the bone marrow, while also pericytes or changes in more invasive phenotype (such as sarcoma-like phenotype) of tumour cells has been studied [21,22,23,24].

Moreover, in the recent years, immunotherapeutic agents have started to have space in RCC [25] and require integration in treatment algorithms and rethinking of the treatment sequence. Immune checkpoint inhibitors activate the immune system against cancer cells; their response pattern may mimic tumour progression, and their class-specific toxicities (immune-related adverse events) include colitis, pneumonitis, and sarcoid-like reaction.

Radiogenomics

Deep research in cancer genomics have spread more and more interest in using the imaging aspects of tumors as a noninvasive surrogate marker of molecular markers, genomic mutations underlying activated biologic pathways, or clinical outcomes finding “association maps” between them, to complement genomic analysis. This is called radiogenomics or radiomics or imaging genomics [26].

The current literature on RCC radiogenomics has focused on ccRCC. Deactivating mutation of the VHL tumour suppressor gene, mutations involving the BRCA1-associated protein 1 (BAP1), polybromo 1 (PBRM1), SET domain containing 2 (SETD2), and lysine (K)- specific demethylase 5C (KDM5C) have been identified [27]. Clinical relevance of these mutation is significant: VHL, PBRM1, BAP1, SETD2, and KD- M5C mutations are shown to be associated with advanced stage disease and poor survival. If we are able to reliably associate imaging features of RCC with mutational status, imaging could play a role in prognostication, treatment selection, and predicting treatment response Mutations of VHL were associated with well-defined tumour margins, nodular tumour enhancement, and intratumoral vascularity, while mutations of KDM5C and BAP1 were associated with renal vein invasion [28]. Mutations of VHL and PBRM1 were also more common among solid ccRCC in this study. BAP1 mutation has been associated with ill-defined tumour margin and presence of calcification, and MUC4 mutation is associated with an exophytic growth pattern [27]. A radiogenomic-based surrogate of molecular assay (SOMA) for multigene signature of ccRCC has been built, using CT image features to noninvasively predict the disease-specific survival independent from stage, grade, and performance status [29]. These efforts represent interesting starting steps in correlating imaging with genetic make-up of RCC.

Thera are some limitation nowadays to the use of radiogenomics, the biggest at present are

limited interobserver agreement in multi-institutional settings, and uncertain generalizability of available data [27]

Morover, validated data are still needed.

Growing interest in tumour texture analysis give a chance to investigators to predict gene expression with the help of new tools. Tumour heterogeneity is a quantifiable feature on images, much like tumour size or attenuation. Tumour heterogeneity can be quantified and used to predict tumour behaviour, response to treatment, and survival, which can help in making management decisions. Texture analysis is essentially an image processing algorithm to extract and quantify tumour heterogeneity. Heterogeneity comes from underlying tumour architecture, from noise due to unequal distribution of photons, and from other technical factors such as peak kilovoltage, use and type of intravenous contrast material, rate of injection. Texture analysis studies several textural parameters of the tumour, sometimes by using filters to focus on areas of variable size in an attempt to enhance true tumour heterogeneity while reducing the effect of photon noise. Heterogeneity is quantified by using parameters such as skewness (a measure of pixel symmetry), kurtosis (measure of “pointedness” of the pixel distribution curve), and entropy (measure of texture irregularity) [30,31]

In a report it has been shown that tumour heterogeneity is an independent factor associated with time to progression of metastatic RCC treated with targeted therapy and can potentially serve as a predictive imaging biomarker of response [31]. Another report has suggested greater heterogeneity of sarcomatoid RCC compared with ccRCC [32].

At present, there are different software and various groups assessed numerous texture parameters using different methods. These texture parameters need to be standardized and validated, the software need to be optimized, and their generalizability needs to be tested. Radiogenomics and texture analysis are new and promising research fields at present focused on the primary tumour; however, it could be interesting to explore the use of these new chances

to look for novel non-invasive biomarker in management of advanced RCC (focusing treatment choice with molecular targeted agents, detection or prediction of response or progression).

Bibliography

1. Reuter VE. The pathology of renal epithelial neoplasms. Semin Oncol. 2006;33:534-543..

2. Amin MB, Amin MB, Tamboli P, et al. Prognostic impact of histologic subtyping of adult renal epithelial neoplasms: an experience of 405 cases. Am J Surg Pathol. 2002;26:281- 291.

3. Motzer RJ, Basch E. Targeted drugs for metastatic renal cell carcinoma. Lancet. 2007;370:2071-2073.

4. Upton MP, Parker RA, Youmans A, McDermott DF, Atkins MB. Histologic predictors of renal cell carcinoma response to interleukin-2-based therapy. J Immunother. 2005;28:488-495.

5. Dutcher JP, Szczylik C, Tannir N, et al. Correlation of survival with tumor histology, age, and prognostic risk group for previously untreated patients with advanced renal cell carcinoma (adv RCC) receiving temsirolimus (TEMSR) or interferon-alpha (IFN) [abstract]. J Clin Oncol. 2007; 25(suppl). Abstract 5033..

6 Lebret T, Poulain JE, Molinie V, et al. Percutaneous core biopsy for renal masses: indications, accuracy and results. J Urol. 2007;178(4 pt 1):1184-1188; discussion 1188.

7. Renshaw AA, Lee KR, Madge R, Granter SR. Accuracy of fine needle aspiration in distinguishing subtypes of renal cell carcinoma. Acta Cytol. 1997;41:987-994

8. Moch H, Cubilla AL, Humphrey PA, Reuter VE, Ulbright TM. The 2016 WHO Classification of Tumours of the Urinary System and Male Genital Organs-Part A: Renal, Penile, and Testicular Tumours. Eur Urol. 2016 Jul;70(1):93-105.

9. Lopez-Beltran A, Scarpelli M, Montironi R, et al. 2004 WHO classification of renal tumours of the adults. Eur Urol. 2006;49:798– 805.

10. Upton MP, Parker RA, Youmans A, et al. Histologic predictors of renal cell carcinoma response to interleukin-2-based therapy. J Immunother. 2005;28:488–9511.

11. Decastro GJ, McKiernan JM. Epidemiology, clinical staging, and presentation of renal cell carcinoma. Urol Clin North Am. 2008; 35:581–92.

12. Pedrosa I, Sun MR, Spencer M, et al. MR imaging of renal masses: correlation with findings at surgery and pathologic analysis. Radiographics. 2008;28:985–1003.

13. rasad SR, Humphrey PA, Catena JR, et al. Common and uncommon histologic subtypes of renal cell carcinoma: imaging spectrum with pathologic correlation. Radiographics. 2006;26:1795–80614.

14. Vargas HA, Chaim J, Lefkowitz RA, et al. Renal cortical tumors: use of multiphasic contrast-enhanced MR imaging to differentiate benign and malignant histologic subtypes. Radiology. 2012;264: 779–88

15. Shinagare AB, Krajewski KM, Braschi-Amirfarzan M, Ramaiya NH. Advanced Renal Cell Carcinoma: Role of the Radiologist in the Era of Precision Medicine.Radiology. 2017 Aug;284(2):333-351

16. Rini BI. New strategies in kidney cancer: therapeutic advances through understanding the molecular basis of response and resistance. Clin Cancer Res 2010;16:1348-54.

17. Albiges L, Choueiri T, Escudier B, et al. A systematic review of sequencing and combinations of systemic therapy in metastatic renal cancer. Eur Urol 2015;67:100-10

18. Fischer S, Gillessen S, Rothermundt C. Sequence of treatment in locally advanced and metastatic renal cell carcinoma. Transl Androl Urol. 2015 Jun;4(3):310-25.

19. Grünwald V, Seidel C, Fenner M, et al. Treatment of everolimus-resistant metastatic renal cell carcinoma with VEGF-targeted therapies. Br J Cancer 2011;105:1635-9

20. Fernando NT, Koch M, Rothrock C, et al. Tumor escape from endogenous, extracellular matrix-associated angiogenesis inhibitors by up-regulation of multiple proangiogenic factors. Clin Cancer Res 2008;14:1529-39

21. Bergers G, Song S. The role of pericytes in blood-vessel formation and maintenance. Neuro Oncol 2005;7:452-64.

22. Jain RK, Booth MF. What brings pericytes to tumor vessels? J Clin Invest 2003;112:1134-6.

23. Rubenstein JL, Kim J, Ozawa T, et al. Anti-VEGF antibody treatment of glioblastoma prolongs surviva but results in increased vascular cooption. Neoplasia 2000;2:306-14.

24 Hammers HJ, Verheul HM, Salumbides B, et al. Reversible epithelial to mesenchymal transition and acquired resistance to sunitinib in patients with renal cell carcinoma: evidence from a xenograft study. Mol Cancer Ther 2010;9:1525-35.

25. Bailey A, McDermott DF. Immune checkpoint inhibitors as novel targets for renal cell carcinoma therapeutics. Cancer J 2013;19:348-52

26. Kuo MD, Jamshidi N. Behind the numbers: Decoding molecular phenotypes with radiogenomics—guiding principles and technical considerations. Radiology 2014;270(2):320–325.

27. Shinagare AB, Vikram R, Jaffe C, et al. Radiogenomics of clear cell renal cell carcinoma:

preliminary findings of The Cancer Genome Atlas-Renal Cell Carcinoma (TCGA- RCC) Imaging Research Group. Abdom Imaging 2015;40(6):1684–1692.

28. Karlo CA, Di Paolo PL, Chaim J, et al. Radiogenomics of clear cell renal cell carcinoma: associations between CT imaging features and mutations. Radiology 2014;270(2):464–471

29. Jamshidi N, Jonasch E, Zapala M, et al. The Radiogenomic Risk Score: construction of a prognostic quantitative, noninvasive imagebasedmolecular assay for renal cell carcinoma. Radiology 2015;277(1):114–123

30. Miles KA, Ganeshan B, Hayball MP. CT texture analysis using the filtration-histogrammethod: what do the measurements mean? Cancer Imaging 2013;13(3):400–406.

31. Goh V, Ganeshan B, Nathan P, Juttla JK, Vinayan A, Miles KA. Assessment of response to tyrosine kinase inhibitors in metastatic renal cell cancer: CT texture as a predictive biomarker. Radiology 2011;261(1):165–171.

32. Schieda N, Thornhill RE, Al-Subhi M, et al. Diagnosis of sarcomatoid renal cell carcinoma with CT: evaluation by qualitative imaging features and texture analysis. AJ

2 – Experimental Section

First Part

Role of MRI DWI sequences in the evaluation of early response to neo-angiogenesis inhibitors in metastatic renal cell carcinoma

With contribution of Prof. A. Vanzulli , Dr. R. Ricotta (ASST grande Ospedale Maggiore Niguarda Ca' Granda, Milano)

Introduction

Neo-angiogenesis is crucial for growth and spread of cancer. Among all factors involved, the Vascular Endothelium Growth Factor (VEGF) is the key point of this process, functioning as target of treatment for many tumours. Therapies with molecular target are characterized by specificity, low toxicity and personalization. Metastatic renal cell carcinoma is nowadays widely treated with VEGF and VEGF-receptor inhibitors, showing substantial antitumor activity and prolonged median progression-free survival [1,2]. Nevertheless, it is still not clear why some patients don't respond.

On the other hand, Response Evaluation Criteria in Solid Tumours (RECIST 1.1) has been widely used to assess tumour response, but these criteria are based on morphological evaluation of changes in gross tumour size and they were primarily designed to control cytotoxic drugs effect. New target agents may alter vascular supply and induce changes in vascularization of lesions before inducing volume reduction; finally, their effect cannot be totally evaluated by RECIST 1.1 [3] and new treatment response criteria to evaluate the effect of target agents are needed.

Recent MRI studies have focused on assessment of functional alteration due to therapeutic response in RCC treated with angiogenesis inhibitors.

DCE-MRI has been widely explored in pre-clinical and clinical studies to assess response to angiogenesis inhibitors [4]. DWI has the potential to explore microstructural information and cell membrane integrity and extracellular space. From previous studies it is known that cell lysis and necrosis determine increase of water diffusion and consequent increase in ADC values [5].

The ability of DWI to identify early therapeutic effects of angiogenesis inhibitors may be of great help in assessing whether treatment is effective or not.

Therefore, the objective of our study was to look for DWI parameters able to identify patients with metastatic renal cell carcinoma who would not benefit from target therapy (angiogenesis inhibitors e.g. Sorafenib and Sutent) in patients with end stage clear cell renal cell carcinoma (ccRCC). RECIST1.1 was assumed as Reference Standard.

Objective of the Study

Our objective was to explore ADC (quantitative parameter of DWI MRI sequencese) as a possible biomarker of treatment response to target agents. In particular we focused on target VEGF – VEGF-R inhibitors (sunitinib & sorafenib) used to treat patients with metastatic renal cell carcinoma (stage IV), considering RECIST 1.1 as reference standard

Material and Methods

Patients Selection and Study Protocol

Our prospective study was approved by the Institutional Review Board and informed consent was obtained from each patient.

From May 2013 to May 2014 consecutive patients with histological proven clear cell Renal Cell Carcinoma (ccRCC) and metastatic disease (Stage IV) were enrolled. Exclusion criteria were (i) patients enrolled in other clinical trials (ii) patients already treated with angiogenesis inhibitors, (iii) any contraindication to MRI. Inclusion criteria were (i) patients eligible to start angiogenesis inhibitors; (ii) with at least 1 target measurable lesion; (iii) measurable lesions at MRI examinations (>2.5 cm). We first select 43 patients, but 2 of them were excluded because they have been already treated with angiogenesis inhibitors, 1 was taking part of another clinical trial, 1 patient didn't have a good target lesion, while 1 patient suffered from claustrophobia. Therefore 38 patients were candidate to start angiogenesis inhibitors and underwent 1,5T MRI examination with multiple b-values DWI sequences (0,40,200,300,600) with the following time-line schedule: t0 MRI, within one week before treatment; t2, 2 weeks after first day of therapy and t8 after 8 weeks from treatment beginning.

During protocol we had to exclude other 5 patients for several reasons: 2 because of lacking of imaging follow-up; 1 because baseline MRI was not qualitative adequate; 2 because of too small lesion at t8 evaluation, not adequate for ADC measure.

Finally, 33 patients with 38 lesions had complete data for comparative evaluation.

Figure 1 shows a flowchart of patient population and study protocol.

Before treatment and after 8 weeks of therapy all patients undergone whole-body CECT, for staging reasons. All patients were finally restaged classifying effectiveness of treatment with RECIST 1.1 criteria, and then subjected to follow-up. Outcome data were available for OS with a follow-up period of 34 months (range 8.3–39.8 months).

Four/33 patients were treated with Sorafenib, 29/33 with Sunitinibe.

In Table 1 are shown clinical characteristics of study population.

MRI Examination and Imaging Post-Processing

All the examinations were performed on clinical 1.5-T MRI scanners (Gyroscan Intera and ACS-NT, 1.5 T; Philips Healthcare, Best, the Netherlands; gradient system: maximum amplitude 30 mT/m, maximum slew rate 150 T/m/s) employing a commercially available 8-element phased array surface receiver coil with the patient in supine position. The same MRI scanner was used in each patient, for baseline and follow up MRI examinations: Baseline MRI (t0) was performed at a mean of 3 days (range 0 – 7 days) before day 1 of the first day of target therapy assumption; MRI after 2 weeks of therapy (t2); MRI after 8 weeks of therapy (t8).

Before DWI, unenhanced T_1 weighted gradient echo (TR=211 ms; TE= 5ms, FOV 350 mm, matrix 256x144, SENSE factor 2, section thickness 8 mm) and T_2- weighted fast spin-echo (TR= 1600 ms, TE=100 ms, flip angle= 80°, FOV 350 mm, matrix 384x196, SENSE factor 2, section thickness 8 mm) axial sequences were acquired.

The DWI sequences consisted of 2 axial free breathing single-shot spin-echo echo-planar imaging variant with 2 different train of *b*-values (*b*0-40-300 and b0-200-600).

Diffusion-weighted signal decay is commonly analysed using the mono-exponential model on a voxel by voxel basis with an implemented algorithm according to the following equation:

$$ADC\ (mm^2\ s^{-1}) = [\ln(S^0 S^b)]/b$$

where S^b is the MRI signal intensity with diffusion weighting b, S^0 is the non-diffusion weighted signal intensity.

ADC value was calculated drawing ROIs on 3 different planes, considering the maximum-diameter-plane and the one upper and below, separately for all b values (b= 40, 200, 300, 600). All measurements were done separately by 2 blinded operators with 5 years and more then 10 years of experience in MRI.

All lesions were measured calculating maximum diameter (following called d=dimension) basing on pre-treatment MDCT and restaging MDCT (performed within 5 days from the t8 MRI), and patients were classified according to RECIST 1.1 criteria [3]:

- Complete Response (CR): Disappearance of all target lesions. Any pathological lymph nodes (whether target or non-target) must have reduction in short axis to <10 mm.
- Partial Response (PR): At least a 30% decrease in the sum of diameters of target lesions, taking as reference the baseline sum diameters.
- Progressive Disease (PD): At least a 20% increase in the sum of diameters of target lesions, taking as reference the smallest sum on study (this includes the baseline sum if that is the smallest on study). In addition to the relative increase of 20%, the sum must also demonstrate an absolute increase of at least 5 mm. (Note: the appearance of one or more new lesions is also considered progression).
- Stable Disease (SD): Neither sufficient shrinkage to qualify for PR nor sufficient increase to qualify for PD, taking as reference the smallest sum diameters while on study.

Patients were then followed up for a median of 39 months and progression free survival (PFS) and Overall Survival (OS) ware assessed.

Statistical Analysis

SPSS, version 20.0 (Chicago, IL) was used for statistical analysis. Inter-observer agreement was assessed with Cohen's Kappa ($k \leq 0.40$ poor agreement, $k = 0.40 - 0.75$ good agreement, $k \geq 0.76$ excellent agreement).

Continuous variables are expressed as mean ± SD.

Effects of treatment on dimension and ADC were explored comparing the same parameter during time (t0 –t2 and t8) and dividing patients in group of response to treatment (PD, DC,

PR), using ANOVA analysis of variance inter- group at the same time and intra-group during time with adjusted F-Test.

Pearson's Correlation Coefficient *r* was used to assess correlations between treatment-induced changes in ADC and in maximum diameter; moreover, it was used to look for correlations between changes in maximum diameter or ADC and PFS or Overall Survival.

A p value <0.05 was considered as statistically significant.

Results

According to RECIST 1.1 criteria, after 8 weeks of treatment, patient were divided in 3 different groups of response: partial response (PR 9/33), stable disease (SD 20/33) and progression disease (PD 4/33). None, as expected, reached complete response (CR).

Average progression free survival was 272 (±252) days, and overall survival of 877 (±705).

Maximum diameter of lesions before treatment (t0) was 40.2±18.2 cm (mean±SD), after 2 weeks of treatment (t2) 38.2±19.8, after 8 weeks of treatment (t8) 35.5±20.6; mean ADC value of lesions at t0, t2 and t8 are shown in Table 2.

An excellent inter-observer agreement was found between the two readers for both maximum diameter and all ADC measurements before treatment, at t2 and t8 (e.g. d t0 k =0,94 and d t8 0,91; ADC b_{600} t0 k=0.84 t8 k=0.88).

Table 2 shows also all results dividing patients by group of response for size (d) and ADC at all b values at t0, t2 and t8.

Differences of size of tumours at t0 among the groups of response show statistically significant results between PR and PD group but not statistically significant differences were found between PD and SD: at T0 patients in PD group have larger tumours than patients on PR group ($p<0.05$).

Looking at the whole population, maximum diameter of tumour didn't have significant change after 2 weeks or 8 weeks of treatment. But as expected in the PD group we found an increase at t8 ($p<0.05$).

Fig.2 shows an example of patients with multiple hepatic lesions.

ADC values for PD, SD, PR groups are graphically shown in fig.3, fig.4.

The differences among the groups of response at t0 is always valid at all b values. Interesting results are found at t0: comparing the 3 different groups at t0, values from b_{40} ADC resulted low for PD, intermediate for DC and high for PR (fig 4).

PR group, as compared to SD or to PD showed higher t0 ADC values at b40 (significant different $p<0.05$): we can assess that more vascularised lesions are more responsive to treatment.

PD group have significantly lower ADC values then both other groups, at t0, t2 and t8, for all b-values except for b_{40} at t8 ($p<0.05$).

ADC at b_{40} patients with PR (group of "responders") showed a previous decrease of mean values (t2) and a following increase after 8 weeks, with values significantly different but lower than t0.

ADC at b_{40} in "non-responders" (PD) shows in contrast a significant increase after 2 weeks and a following reduction, with statistically significant higher values than t0.

ADC at b_{200}, b_{300} and b_{600} show some changes in all groups of response, but this seems not to have a univocal trend of change useful to differentiate responders from non-responders.

Correlations of PFS and OS with all parameters were calculated, some of them poor and not statistically significant (Table 3). However, some results were interesting:

- First of all, size of lesions at t0 doesn't correlate significantly with PFS or OS (respectively r=0,14 and r=0,29 for maximum diameter);
- ADC t0 b_{40} showed better results than dimension and the best result of significant correlation with overall survival (respectively with PFS and OS r=0,30 and r=0,62 for ADC b_{40});
- ADC t0 at the other b-values shows no significant results, but a trend of positive correlation as compared to d t0, in some occasion even better than d (e.g. b600 & PFS r=0,32; b300 & OS r=0,34);
- Changes in ADC b_{40} (expressed as percent of changes from t0 to t2 and from t0 to t8) have some interesting inverse correlations with PFS and OS; the correlation with OS is slightly higher for ADC than for dimensional criteria (respectively for $\%\Delta_{ADC}$ t0-t2 and $\%\Delta_{ADC}$ t0-t8 r=-0,44 and r=-0,42; $\%\Delta_d$ t0-t2 and $\%\Delta_d$ t0-t8 r= -0,11 and r=-0,39): changes

of ADC b_{40} after only 2 weeks of treatment achieve and slightly overcome the dimensional criteria (either expressed as $\%\Delta_d$t0-t2 or $\%\Delta_d$t0-t8) in predicting overall survival;

- Surprisingly very low correlations with PFS and OS were found looking at b_{600} ADC changes at t2, while after 8 weeks (t8) a slight positive correlation was found between changes of ADC and PFS (r=0.36).

Discussion

Angiogenesis is essential for the progression of all solid tumours, and angiogenesis inhibition remains a promising approach in cancer therapy. The antiangiogenic agent we used, sorafenib and sunitinib, are orally active multi-kinase inhibitors with effects on VEGF receptors, platelet-derived growth factor receptors and tyrosine kinase [6].

They are currently approved for advanced hepatocellular carcinoma and RCC and has been shown to have significant clinical activity: the life expectancy of RCC patients has been extended to over 30 months [7]; moreover, it has been shown prolonged progression-free survival in patients with metastatic RCC in whom previous systemic therapy had failed [1,2]

However, a significant portion of patients with advanced RCC inevitably develop resistance to angiogenesis inhibitors and relapse, likely for a mechanism derived from a non-VEGF-mediated angiogenesis escape [8].

The possibility to determine the development of VEGF-inhibitors resistance at an early time point is very important, since these patients can be shifted to second and third line therapies. In particular this is important for patients who can benefit from new immunotherapy agents.

Traditionally response assessment in cancer patients was found on size- based tumor response criteria and revised RECIST criteria are the most commonly used method for RCC (RECIST 1.1). However, limitations of its use in modern RCC treatment are known, and include lack of early indicators of response, lack of validation for use in novel targeted agents, and exclusion of advanced imaging techniques information [44]

In the other hand it is crucial to find a ready to use, simple, repeatable and not invasive way to select patients potentially non-responders before or at the very beginning of therapies, because RECIST criteria (with 1.1 version) are by now not enough. Use of contrast media, even if seems to be interesting (but far to be perfect) in DCE- MRI (quantitative parameters such as K_{trans}; v_e) [10,11], is not free from risks, especially in patients with chronic renal insufficiency, since the

exam has to be repeated at least every 2 weeks during the first cycles of target therapies to possibly select early non-responders. CT texture analysis is a relatively new tool for exploring new image characteristics based on pixel HU and histogram statistical analysis of a ROI [12,13]; it has good potential, but it hasn't been used for assessing RCC response to target therapy yet.

DWI and ADC maps can be interesting in this field, because, excluding patients with absolute contraindications on performing MRI, it is a safe, repeatable and fast method, that doesn't expose patients to any particular risk.

Therefore, we investigated the feasibility of DWI in monitoring early tumour response to sorafenib or sunitinib in patients with metastatic clear cell Renal Cell Carcinomas (ccRCC), looking for a parameter (ADC) potentially able to predict response to angiogenesis- inhibitors, before starting treatment or early after day 1. RECIST 1.1 criteria were considered the reference standard for comparison.

The application of this MR technique to RCC after angiogenesis inhibitors treatment has already been attempted in few articles.

Desar et All [14] evaluated the mean ADC values within a single slice through the primary renal tumour at three time points (baseline, day 3 and day 10 of the first treatment cycle) in ten patients treated with sunitinib. They demonstrated chemotherapy-related changes in mean ADC, which were attributed to cellular swelling at day 3 (increased mean ADC) followed by tissue dehydration by day 10 (reduction in mean ADC compared with day 3). These ADC changes did not correlate with DCE-MRI parameters or response measures (outcome) in their patient group.

Bharwani et All [15] evaluated DW-MRI of 26 patients with metastatic RCC treated with sunitinib before and after 3 cycles, generating whole-tumour apparent diffusion coefficient (ADC) maps and histograms. They showed that patients with a greater proportion of tumour lying below the 25th percentile point of the whole-tumour ADC histogram (a greater proportion

of restricted tissue) at t0, had reduced survival. In addition, patients with a greater-than-median positive change in AUC_{low} (i.e., an increase in the proportion of restricted tissue) had reduced survival, whereas those with a decrease in AUC_{low} had prolonged survival. These seems to be quite interesting results, but the method is complicated and not easily and routinely reproducible.

Looking at other solid tumours Orton et All [16] recently evaluated diffusion MR imaging of metastatic abdominal and pelvic tumours in patients treated with VEGF-inhibitors, using alternative attenuation model. They found significant increase in the diffusion coefficients from all models at day 28 but not at day 7. They also observed weak correlations between DW-MRI changes and volume changes.

That's why we focused on a practical approach to the ADC evaluation, trying to understand if we can find an outcome predictor in the simplest way of calculating ADC. This is the reason why we decided to perform free-breathing DWI sequences, no contrast agents, and a post processing 2D ROI evaluation, even knowing the limitations of the method.

Results show that patients with early progression (PD at t8) have significantly lower ADC values than PR or DC every-time (t0, t2, t8). We could explain this result saying that these patients have lesions with more necrosis, less vascularization and more cellularity (low ADC values at b_{40}-b_{600}) and they don't respond to angiogenesis inhibitors. This is quite interesting and if confirmed by other Authors can become a biomarker of potentially lack of response to target agents before starting target therapies.

Changes in ADC after therapy surprisingly were confusing and without a univocal trend in comparison with previous studies. But looking at the graphic of comparison of the 3 group of response we can say that in our cohort of patients the single measure at t2 or t8 has not a significant meaning but the change of ADC (b_{40}) at t2 as compared to t0 (delta t0- t2) has good

potential to distinguish patients: patients that respond have an early reduction of ADC, stable patients have no reduction, while patient with early progression have a paradoxical increase of ADC. Caution to interpret these data is mandatory, since our best results comes from very low b values, in which effects of microscopic perfusion and diffusion are similarly contributing to the grey-scale-encode intensity of each voxel, and so can be considered as a "perfusion surrogate" rather than diffusion parameter.

We didn't look for a cut off value because of the small number of patients. Moreover, it is difficult to talk about precise values in ADC, because they are machine dependant, sequence dependent and patient dependent. Anyway the trend is interesting and probably giving the same MRI machine and the same pathology it will be possible in the future to identify precise values.

Looking at outcome parameters, we had enough data to correlate our ADC parameters and PFS or OS.

First, interestingly PFS correlate with OS in our cohort of patients. It is known that patients with metastatic renal cell carcinoma at the beginning start responding to the VEGF-inhibitors, but sooner or later they relapse. This is due to molecular mechanism of resistance, with activation of new pat-ways of regulation of angiogenesis. Literature says that the time to new progression is not necessarily correlated with final outcome [17]. In our group of patients, we found good correlation of PFS with OS, highlighting that the sooner our patients relapse, the sooner they die.

Moreover, early cellular swelling and decreased vascularity induced by therapy after 2 weeks may lead to a transient decrease in ADC value in patients that respond effectively to treatment (PR group).

At t0 there is a better correlation between PFS & ADC (b_{40}) then PFS & dimensional criteria. This is important, because confirm that lesions with higher ADC b_{40}, having higher vascularity, have more chance to respond to VEGF inhibitors and confirm that dimensional criteria of

response evaluation (RECIST), with the advent of target therapy, are not anymore as useful as in the past era of cytotoxic conventional chemotherapy.

There are some limitations to the present study, the first is the small group of patients. We had a small number of patients in PD group and this could have biased our results. Secondly, we analysed lesions differently located in abdomen, mediastinum and pelvis, knowing that this could affect DWI and ADC measurements.

Conclusion

Nowadays, in the era of target therapy, it is crucial to select patients who potentially can benefit of target agents. We have to look at possible new treatment options and to cost/benefit ratio, as well as avoid patient’s subject to unnecessary side effects related to the treatment.

ADC at t0 may help selecting patients with promising good response to angiogenesis inhibitors. Moreover, at t0 and at t2 ADC has the potential to select patients who wouldn't benefit from angiogenesis inhibitors. These results come from low b-values and confirm that pre-assessment of grade of vascularity of the lesion can be of great help in treatment decision making.

DWI has the potential role to identify patients whose tumour wouldn’t benefit from target therapy, adding a value (ADC) to other imaging (e.g. DCE-MRI, texture imaging) and genomics parameters (e.g. miRNA) in a hypothetic multi-parametric analysis, with a possible future radiogenomics approach.

Figure 1

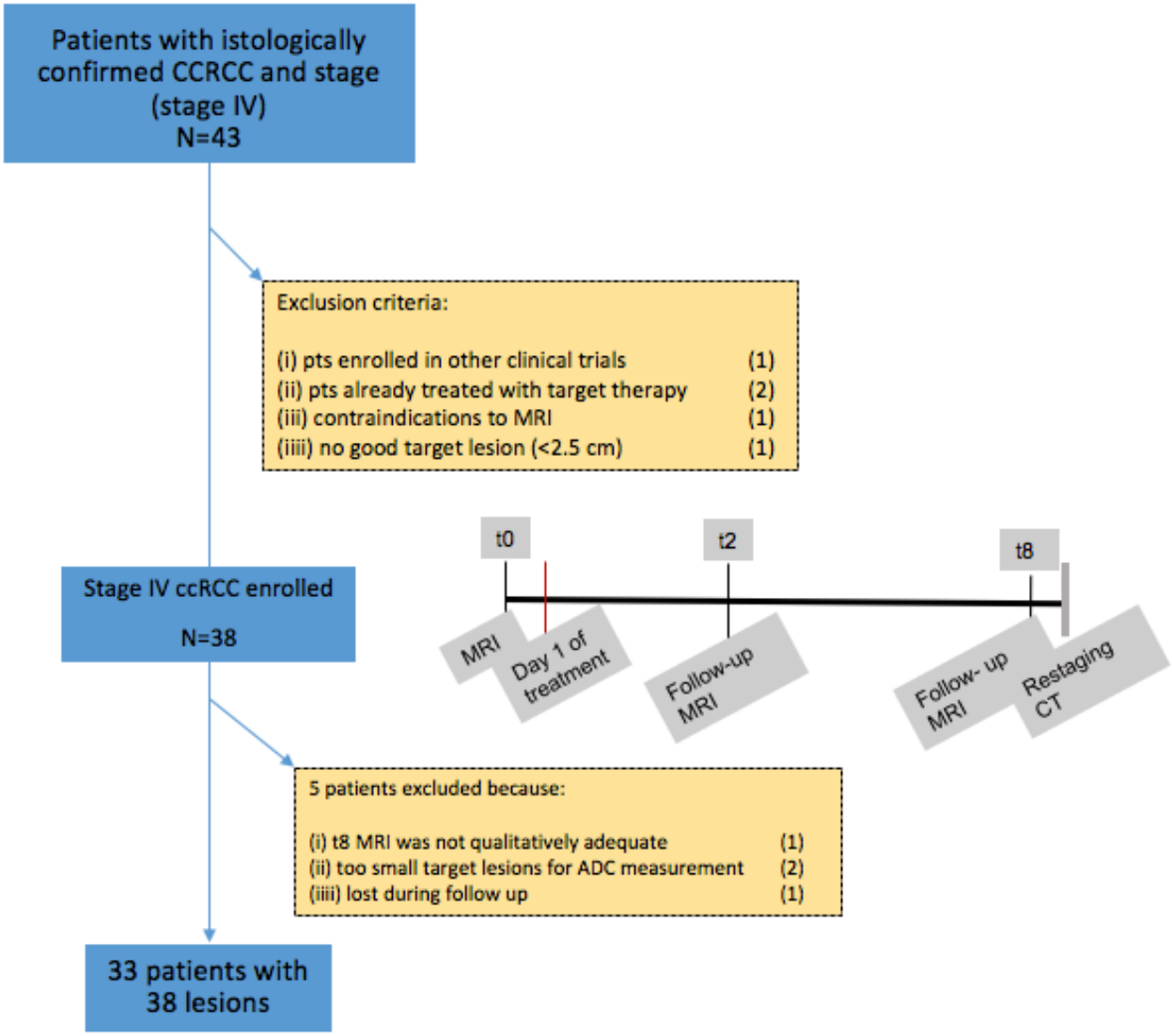

Fig. 1 Flowchart of patients and protocol of the study

Table 1

Patient demographics and characteristics at diagnosis	
Number of patients	33
Age (years)	65,7±5,8
Gender	
Male	22
Female	11
Lesions	
Adrenal	7
Liver	9
Peritoneum	2
Retroperitoneum	4
Ab. lynphnodes	5
Lung	1
Mediastinum lynphnodes	2
Soft tissue	3
Bone	1
Kidney	4
Treatment	
Sorafenib	4
Sunitinib	29
Line of treatment	
1	20
2	13
MSKCC prognostic risk	
Intermediate	23
Poor	10
Clear cell tumour grade	
1-2	9
3-4	24
Median OS, months	29 (±23)
Median PFS, months	9 (±8)
Abbreviations: MSKCC= Memorial Sloan-Kettering Cancer Centre; OS=overall survival; PFS=progression-free survival	

Tab. 1 Demographics and characteristics of patient's population

Table 2

N=33	ADC b40	ADC b200	ADC b300	ADC b600	d
t0	4,05±1,14	2,25±0,45	2,05±0,36	1,72±0,19	40,2±18,2
t2	3,69±1,20	2,00±0,40	1,96±0,29	1,60±0,19	38,2±19,8
t8	3,55±1,07	1,96±0,32	1,90±0,28	1,56±0,15	35,5±20,6

a)

PR	ADC b40	ADC b200	ADC b300	ADC b600	d
t0	6,85±1,17	2,14±0,37	2,79±0,45	1,93±0,17	38,5±14,8
t2	3,86±1,46	2,51±0,35	2,12±0,27	1,84±0,15	32,8±16,8
t8	4,89±1,26	1,87±0,37	2,51±0,30	1,59±0,16	20,4±4,2

b)

SD	ADC b40	ADC b200	ADC b300	ADC b600	d
t0	3,56±1,15	2,37±0,50	1,96±0,34	1,74±0,19	37,8±26,3
t2	3,59±1,08	1,89±0,41	1,99±0,29	1,49±0,20	37,5±25,6
t8	3,17±1,02	2,06±0,31	1,77±0,27	1,63±0,15	35,4±23,0

c)

PD	ADC b40	ADC b200	ADC b300	ADC b600	d
t0	1,73±0,98	1,64±0,26	1,29±0,32	1,14±0,22	44,5±13,4
t2	4,10±1,52	1,24±0,25	1,44±0,30	0,97±0,12	53,0±22,6
t8	3,43±1,08	1,21±0,29	1,32±0,30	0,82±0,15	57,5±27,6

d)

Tab.2 ADC median values and dimensions (d, cm) at different b values during follow-up. a) all patients are considered together; b) Partial Response group (PR); c) Stable Disease group (SD); c) Progression Disease group (PD)

Figure 2

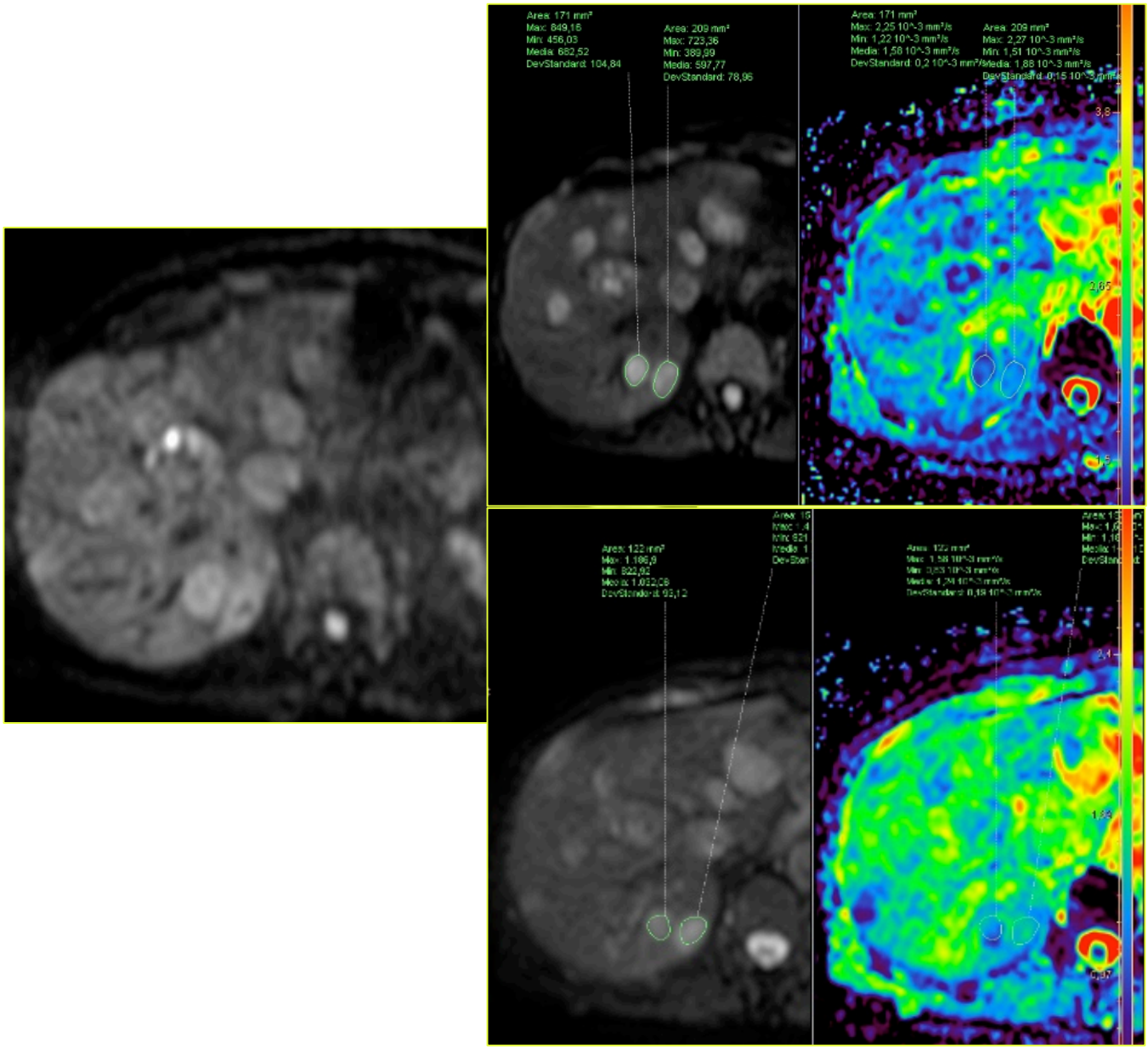

Figure 2 Example of ADC maps elaborated from DWI at b40 (upper) and at b600 (lower) in a patient with multiple hepatic lesions. Lesions are slightly hyperintense. ROI are manually drawn on the lesions (e.g. 2 lesions on S7) and Mean ADC value is provided

Figure 3

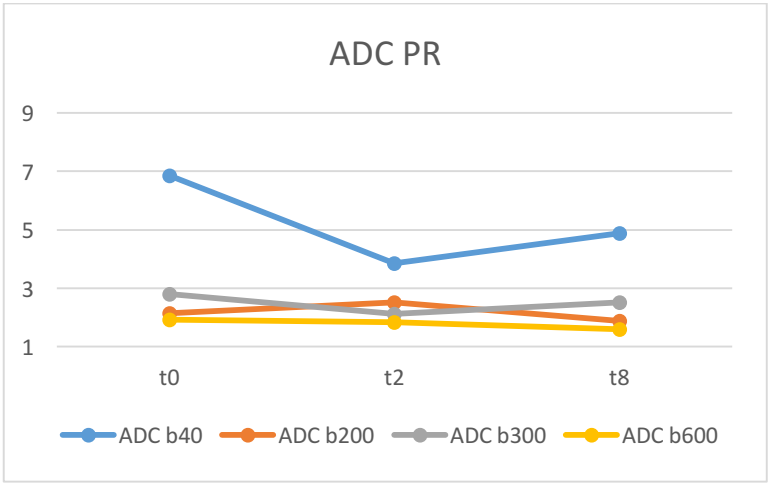

a)

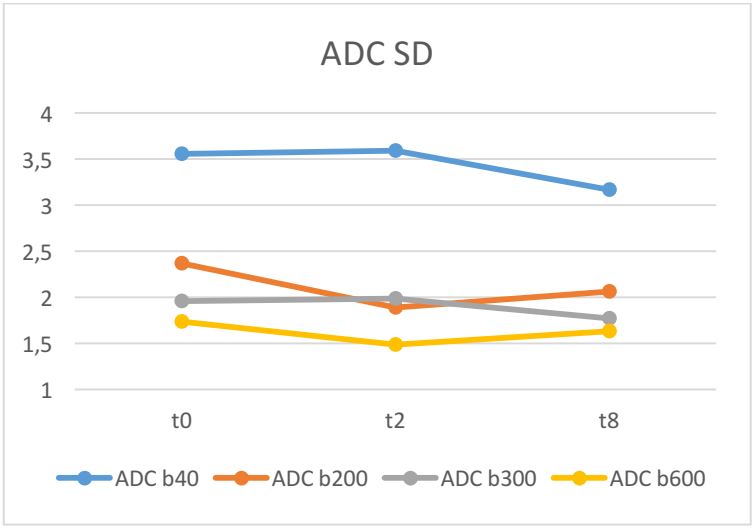

b)

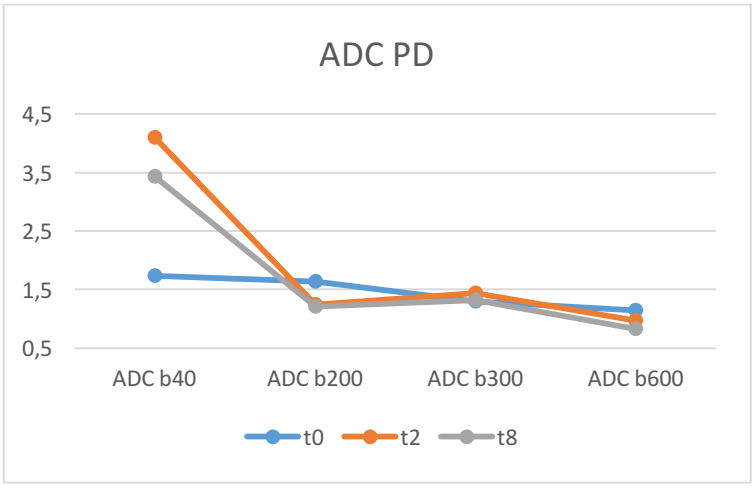

c)

Fig. 3 of ADC for all b values in a) partial response group; b) stable disease group; c) progression disease group

Figure 4

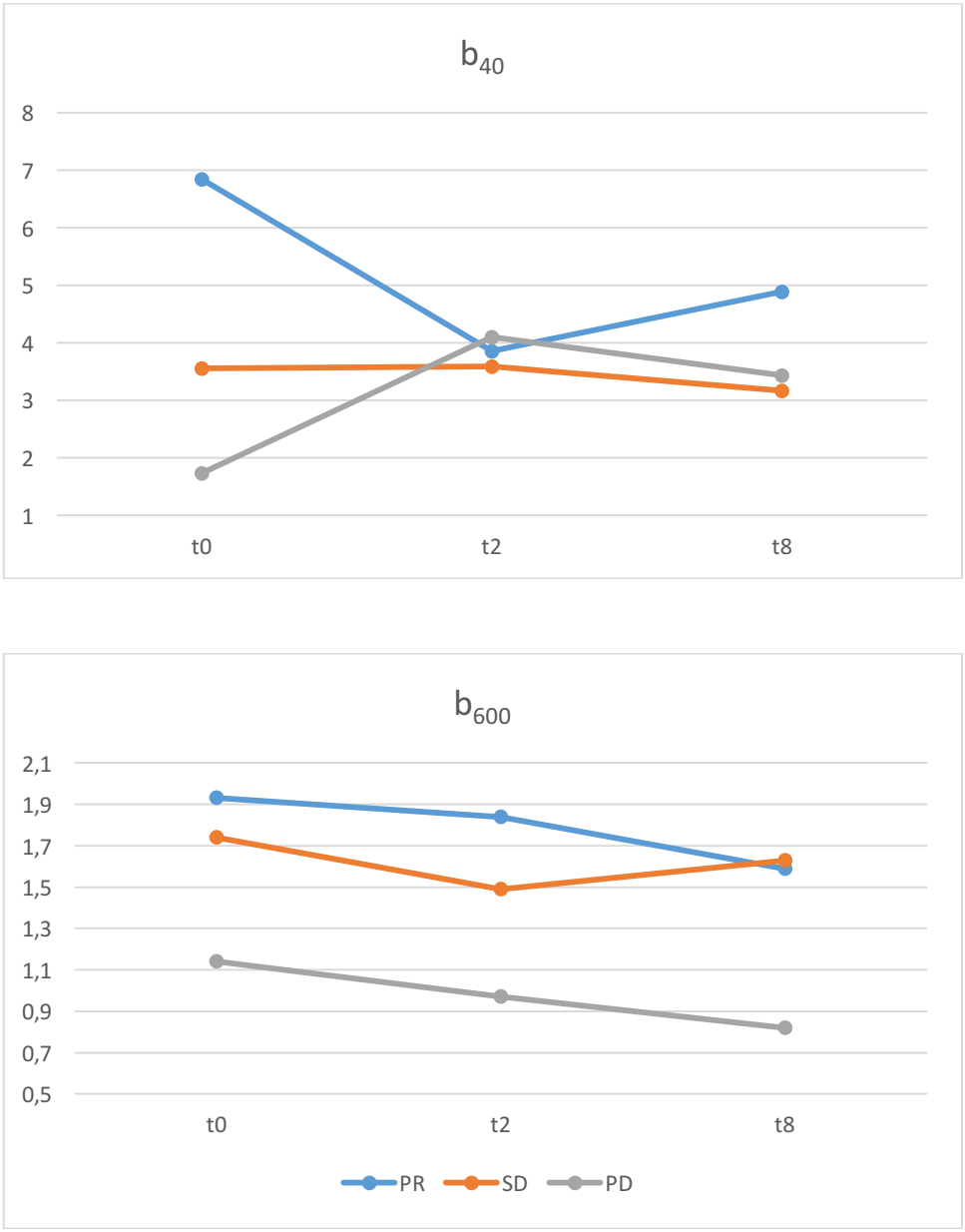

Fig.4 Comparison of group of response: ADC b_{40} (a) and b_{600} (b) at t0, t2, t8.

Table 3

dimension	PFS	OS
Δ (%) d t0-t2	-0.33*	-0.11
Δ (%) d t0-t8	-0.58*	-0.39*
d t0	0.14	0.29

a)

b40	PFS	OS
Δ(%) ADC t0-t2	-0.26	-0.42*
Δ(%) ADC t0-t8	-0.16	-0.44*
ADC t0	0,30	0.62*
ADC t2	0,18	0.20
ADC t8	0.29	0.29

b)

b300	PFS	OS
Δ(%) ADC t0-t2	-0.08	-0.7
Δ(%) ADC t0-t8	-0.02	0.04
ADC t0	0.23	0.34
ADC t2	0.19	0.29
ADC t8	-0.04	-0.02

c)

b600	PFS	OS
Δ(%) ADC t0-t2	-0.12	-0.15
Δ(%) ADC t0-t8	0,36*	-0.9
ADC t0	0,32	0.19
ADC t2	0,23	0.33
ADC t8	0.17	0.10

d)

Tab. 3 Pearson Correlations between Dimensional criteria (**a**) or ADC (**b, c, d**) with Progression Free Survival and Overall Survival. * indicates statistically significant results ($p>0.05$). Best results are found for ADC at b_{40} (**b**)

Bibliography (References)

1. Escudier B, Eisen T, Stadler WM, Szczylik C, Oudard S, Siebels M, et al; TARGET Study Group. Sorafenib in advanced clear-cell renal-cell carcinoma. N Engl J Med 2007; 356: 125–34..

2. Kane RC, Farrell AT, Saber H, Tang S, Williams G, Jee JM, et al. Sorafenib for the treatment of advanced renal cell carcinoma. Clin Cancer Res 2006; 12: 7271–8.

3. Eisenhauer EA, Therasse P, Bogaerts J, Schwartz LH, Sargent D, Ford R, Dancey J, Arbuck S, Gwyther S, Mooney M, Rubinstein L, Shankar L, Dodd L, Kaplan R, Lacombe D, Verweij J. New response evaluation criteria in solid tumours: revised RECIST guideline (version 1.1). Eur J Cancer. 2009 Jan;45(2):228-47

4. Hahn OM, Yang C, Medved M, Karczmar G, Kistner E, Karrison T, et al. Dynamic contrast-enhanced magnetic resonance imaging pharmacodynamic biomarker study of sorafenib in metastatic renal carcinoma. J Clin Oncol 2008; 26: 4572–8.

5. Padhani AR, Liu G, Koh DM, Chenevert TL, Thoeny HC, Takahara T, et al. Diffusion weighted magnetic resonance imaging as a cancer biomarker: consensus and recommendations. Neoplasia 2009; 11: 102–25.

6 Wilhelm SM, Carter C, Tang L, Wilkie D, McNabola A, Rong H, et al. BAY 43-9006 exhibits broad spectrum oral antitumor activity and targets the RAF/MEK/ERK pathway and receptor tyrosine kinases involved in tumor progression and angiogenesis. Cancer Res 2004; 64: 7099–109.

7. Motzer RJ, Barrios CH, Kim TM, et al. Phase II randomized trial comparing sequential first-line everolimus and second-line sunitinib versus first-line sunitinib and second-line everolimus in patients with metastatic renal cell carcinoma. J Clin Oncol 2014;32:2765 -72

8. Sosman JA, Puzanov I, Atkins MB. Opportunities and obstacles to combination targeted therapy in renal cell cancer. Clin Cancer Res 2007; 13: 764s–9s.

9. Liu Y, Litière S, de Vries EG, et al. The role of response evaluation criteria in solid tumour in anticancer treatment evaluation: results of a survey in the oncology community. Eur J Cancer 2014;50(2):260–266

10. Flaherty KT, Rosen MA, Heitjan DF, et al. Pilot study of DCE-MRI to predict progression free survival with sorafenib therapy in renal cell carcinoma. Cancer Biol Ther 2008;7(4):496–501

11. Hahn OM, Yang C, Medved M, et al. Dynamic contrast-enhanced magnetic resonance imaging pharmacodynamic bio- marker study of sorafenib in metastatic renal carcinoma. J Clin Oncol 2008;26(28): 4572–4578.

12. Miles KA, Ganeshan B, Hayball MP. CT texture analysis using the filtration-histogram method: what do the measurements mean? Cancer Imaging 2013;13(3):400–406

13. Goh V, Ganeshan B, Nathan P, Juttla JK, Vinayan A, Miles KA. Assessment of response to tyrosine kinase inhibitors in metastatic renal cell cancer: CT texture as a predictive biomarker. Radiology 2011;261(1):165–171

14. Desar IM, ter Voert EG, Hambrock T, van Asten JJ, van Spronsen DJ, Mulders PF, Heerschap A, van der Graaf WT, van Laarhoven HW, van Herpen CM. Functional MRI techniques demonstrate early vascular changes in renal cell cancer patients treated with sunitinib: a pilot study. Cancer Imaging. 2012 Jan 12;11: 259-65.

15. Bharwani N, Miquel ME, Powles T, Dilks P, Shawyer A, Sahdev A, Wilson PD, Chowdhury S, Berney DM, Rockall AG. Diffusion-weighted and multiphase contrast-enhanced MRI as surrogate markers of response to neoadjuvant sunitinib in metastatic renal cell carcinoma. Br J Cancer. 2014 Feb 4;110(3):616-24.

16. Orton MR, Messiou C, Collins D, Morgan VA, Tessier J, Young H, deSouza N, Leach MO. Diffusion-weighted MR imaging of metastatic abdominal and pelvic tumours is sensitive to early changes induced by a VEGF inhibitor using alternative diffusion attenuation models. Eur Radiol. 2016 May;26(5):1412-9

17. R Amir E, Seruga B, Kwong R, Tannock IF, Ocaña A. Poor correlation between progression-free and overall survival in modern clinical trials: are composite endpoints the answer? Eur J Cancer. 2012 Feb;48(3):385-8.

Second Part

CT Texture Analysis in Clear Cell Renal Cell Carcinoma: a Radiogenomics Prospective

With contribution of Prof. V. Petrozza(1), Dr. F. Fazi (2) , Dr. G. Bellotti(3), Dr. S. Badia (3), Prof. A. Laghi (3) (1) Pathology Unit, ICOT, Department of Medico-Surgical Sciences and Biotechnologies, Sapienza University of Rome, Latina 04100, Italy; vincenzo.petrozza@uniroma1.it(2) Department of Anatomical, Histological, Forensic & Orthopaedic Sciences,

Section of Histology & Medical Embryology, Sapienza University of Rome, Rome 00161, Italy;(3) Università Roma Tre (4) ICOT Department of Radiology

Introduction

Clear cell Renal cell carcinoma (ccRCC) is a common group of chemotherapy-resistant tumour representing 2%–3% of adult malignancies, with the clear cell histotype (ccRCC) accounting for 80%–90% of all RCCs [1]. It is the third most common urological cancer after prostate and bladder cancer, but it has the highest mortality rate (about 40%) [2]. Deeper molecular characterization could improve ccRCC diagnosis and management, as well as prognosis and treatment choice. In this scenario miRNA are emerging as interesting biomarkers for several tumours [3] [4]. They are small noncoding RNAs which have an important role in the regulation of carcinogenesis pathways: pathological tissue expresses miRNAs in a different way compared with corresponding normal tissue, regulating important breakpoints during carcinogenesis [5] [6]. Recently they have been addressed as part of ccRCC tumorigenesis and progression [7] [8], so that a “miRNA signature” in ccRCC has been described and significantly correlated with

patient outcome [9] [10]. miR-21 and miR-210 as well as miR-185 and miR-221 showed functional relevance for ccRCC tumorigenesis [11] [12].

The grade of expression of miRNAs is cancer- and tissue-specific and often it’s in accordance with tumour’s grading; for this reason expression profile of miRNA in ccRCC can be helpful to differentiate healthy from pathological tissue, to identify slightly differentiated cancers that would otherwise be undetermined with the use of conventional histology and immunohistochemistry and, lastly, to recognize tumours with different histotype within the same organ [5].

Going further we tried to understand if the “ccRCC miRNA signature” had a corresponding phenotype in radiological examinations (radio-phenotype), looking for a connection between genotype and radio-phenotype, in a radiogenomics point of view.

An emerging potentially useful imaging biomarker is CT tumour texture analysis (CTTA), which has shown promising results in predicting patient outcome, overall survival and response to therapy for multiple RCC histotypes. [13] [14]

CTTA is a quantitative technique that allows to characterize the heterogeneity of a lesion inside a region of interest (ROI) by analysing the distribution and relationship of pixel grey-levels using both unfiltered and frequency filtered images, deriving quantitative texture parameters based on attributes of the pixels and the image histogram.[13].

Objective of the Study

To the best of our knowledge, none has investigated a possible correlation between CT texture parameters and miRNA expression in ccRCC.

For this reasons, the aim of this study was to investigate whether quantitative parameters obtained from CTTA correlate with different grade of expression of mi-RNA in patients affected by clear cell Renal Cell Carcinoma (ccRCC).

Material and Methods

This retrospective, single-centre, Health Insurance Portability and Accountability Act-compliant study was approved by the Institutional Review Board and informed consent was obtained.

No authors are employees of or consultants for industry or had control of inclusion of any data and information that could represent a conflict-of-interest. There was no industry support specifically for this study.

Study Population

Figure 1 portrays the subjects' accrual flowchart, which is based on the Standards for Reporting of Diagnostic Accuracy (STARD) initiative. Forty-five consecutive patients who underwent contrast enhanced computed tomography (CECT) of abdomen and pelvis for suspected ccRCC between April 1, 2014 and June 1, 2016, were primarily included. Clinical indications for CT included (*i*) clinical suspicion for ccRCC cancer based on the patient's clinical history and/or elevated tumour markers levels or (*ii*) patients known to have a suspicious renal lesion on the basis of the results of prior imaging studies, such as ultrasonography, unenhanced CT, or magnetic resonance (MR) imaging. Subjects were considered not eligible for this study if (*i*) the CT examination resulted in no kidneys lesions; (*ii*) patients underwent previously chemotherapy, radiotherapy or immunotherapy; (*iii*) too small lesion for good CTTA analysis (<2 cm), (iv) inadequate image quality due to either suboptimal injection technique, poor timing for the acquisition of the urographic phase, or deviations from the routine CT protocol (e.g., inappropriate selection of kV or reconstruction kernel by the CT technologist). Basing on CT and clinical pre-surgery evaluations we could include 35 patients, 8 of which were proved to have benign lesions (basing on other imaging evaluations, follow up, percutaneous biopsy). Finally, two patients with suspicious RCC on the base of CT characteristics refused biopsy or surgery due to old age and suboptimal global clinical conditions. Thirty-one patients underwent

biopsy (5/31) or direct surgery (26/31 nephrectomy or tumorectomy basing on tumour size). After histopathological examination only 21 clear cell renal cell carcinoma were found; one of them was not eligible for the study because of no complete miRNA extraction for tumour and matched normal tissue.

Our final study population included 20 patients (14 males, 6 females; mean age 65 years ± 13, range 35-87 years; mean Body Mass Index (BMI) 27 kg/m^2 ± 4,37; range 20,8-40,3 kg/m^2) with 20 ccRCC suitable for Texture analysis CT examination and miRNA extraction (Table 1).

Hystopatological Analysis (RNA Extraction and MicroRNA Expression Analysis)

Eight samples of fresh frozen tissues from 8 ccRCC lesions were analysed and homogenized by gentle dissociator (Miltenyi Biotec) in 700 microl of Qiazol (Qiagen, Chatsworth, CA); RNA was extracted using manufacturer's instructions.

A cohort of 12 ccRCC formalin-fixed paraffin-embedded (FFPE) tissue samples from 12 patients was analysed. RNA was extracted using the miRneasyr FFPE kit (Qiagen, Chatsworth, CA, USA) following the manufacturer's instructions.

For each sample, a matched normal tissue sample was collected.

For both cohorts, the concentration and purity of total RNA were assessed using a Nanodrop TM 1000 spectrophotometer (Nanodrop Technologies, Wilmington, DE, USA). A quantity of 150 ng of total RNA was reverse transcribed in 8 μL using miScript II RT kit (Qiagen, Chatsworth) and 1 μL of cDNA dilution (1:4) was used for quantitative real time PCR (RT-qPCR) experiments. PCR quantification analysis of the SCARNA17 SNORD61, SNORD68, RNU6-2 and miRNAs miR-21-5p, miR-210-3p, miR-185-5p, miR-221-3p and miR-145-5p, was performed using the miScript SYBR Green PCR kit (Qiagen, Chatsworth) with the miScript Primer Assay Hs-SCARNA17 (#MS00014014), SNORD61 (#MS00033705), SNORD68 (#MS00033712), RNU6B-2 (#MS00033740), Hs-miR-21-5p (#MS00009079), Hs-miR-210-3p (#MS00003801), Hs-miR-

185-5p (#MS00003647), Hs-miR-221-3p (#MS00003857), Hs-miR-145-5p (#MS00003528) (Qiagen, Chatsworth, CA, USA).

The expression analyses of RNU19 and RNU66 were performed by TaqMan MicroRNA RT assay and TaqMan MiRNAr Assays (RNU19 #001003 and RNU66 #001002) (Applied Biosystems, Foster City, CA, USA) according to the manufacturer's protocol. All reactions were performed in duplicate. Data were analysed by quantification relatively to a standard curve. The standard curve was prepared with serial dilutions of a reference cDNA obtained from RNA extracted from a tumour sample. z-scores were calculated for all expression values to standardize the data. Subsequently, z-score values of RNU66, RNU19 and SCARNA17 were averaged and used to normalize the expression values of each miRNA in FFPE samples while z-score values of SNORD61, SNORD68, RNU6-2 were averaged and used to normalize the expression values of each miRNA in fresh frozen samples.

MDCT Acquisition Protocol

All scans were performed with a 64-row multiple detector computed tomography (MDCT) scanner (Lightspeed VCT®, GE Medical Systems, Waukesha, WI, USA) using the following parameters: kV, 120; beam pitch, 1.375:1; detector configuration, 64×0.625 mm; reconstructed section thickness, 1.25 mm.

A z-axis tube current modulation was used, with a noise index of 28 (min/max mA: 200/600) which was recommended by the manufacturer for standard abdominal CT in all cases. All examinations were performed using a multiphase MDCT protocol (Table 2).

All patients received an average of 120 mL of an intravenous non-ionic contrast medium with an iodine concentration of 350 mg iodine/mL (Iomeprol®, Iomeron 350®; Bracco, Milan, Italy). The bolus of contrast medium was injected through an 18-20 gauge cannula inserted into an antecubital vein using a dual-chamber peristaltic injector (CT Exprès®, Bracco, Milan, Italy) at a flow rate of 3,5 mL/s.

All patients were positioned supine with head first on the scanning table. The scanning protocol started with the acquisition of anteroposterior and lateral digital localizer radiographs. The acquisitions of the abdomen and pelvis were performed in the cranio-caudal direction after iodine intravenous injection of contrast medium in arterial, portal, equilibrium and urographic phases.

A bolus tracking technique was used to minimize the influence of cardiac output; CM detection was monitored in a region of interest (ROI) placed in the aorta at the level of the diaphragm; the threshold for the start of the scan was set at 100 HU. A late arterial phase was acquired 18 s after reaching the threshold; a portal phase 35 s after the end of arterial phase; an equilibrium phase was acquired at 120 s after the end of portal vein and urographic phase was acquired after 12 minutes.

Image Reconstruction

Imaging reconstructions were obtained using 40% of an iterative reconstruction algorithm (ASiR®, GE Healthcare, Milwaukee, WI, USA).

Images were reconstructed using a medium-smooth kernel (Q30) at 1.25-mm reconstructed section thickness (Table 2).

Imaging Data Analysis

All analyses were performed using a commercially available CTTA research software platform (Version 1.1; TexRAD Ltd®, Somerset, UK) on a dedicated workstation. CTTA was performed on twenty clear renal cell carcinomas (RCCs) drawing manually two different polygonal ROIs at three different axial levels in arterial, portal, delayed and urographic phases (Fig. 2): 1) into the lesion (including the majority of the lesion in that plane and excluding margins); 2) in the normal parenchyma of the kidney including cortical and medullar layers.

All images were reviewed, and slices were selected by two readers (radiologist with 10 years of experience and radiology resident with 3 years of experience on abdominal CT).

The technique consisted of a preliminary filtration step, followed by quantification of the texture within the filtered images.

The filtration step comprised Laplacian of Gaussian (LoG) spatial band-pass filter used to produce multiple series of derived images extracting and enhancing features at different anatomical spatial scales; this resulted in a series of derived images from fine to coarse texture within a region of interest (ROI) identified with “spatial scaling factor” (SSF). The scale was selected by tuning the filter parameter between 0 and 2.0, where SSF1.0 indicates fine texture (features of approximately 2 pixels in width), SSF1.5, 1.8 and 2.0 indicate degrees of medium textures (features of approximately 6, 8 and 10 pixels in width respectively).

This is followed by quantification of statistical parameters in a histogram-based statistical approach (first, second or higher order parameters). The software output includes: mean pixel attenuation (M, Mean), standard deviation of the pixel distribution histogram (SD, dispersion from the mean), entropy (E, irregularity in terms of randomness of distribution of pixels), mean of positive pixels (MPP), skewness of the pixel histogram (S, asymmetry), kurtosis (K, sharpness) of the pixel histogram, and the percentage of positive pixels; all these histogram – based parameters are provided for each spatial scaling factor.

Statistical Analysis

All data were described as mean ± standard deviation.

CTTA was performed for each of the six parameters at each SSF (in number of 5) and for all post-contrast CT phases acquired (i.e. healthy kidney, arterial phase, portal phase and urographic phase), with a total of 120 variables.

A matrix of data on MatLab® has been elaborated from 5 different miRNAs (miR-145-5p, miR-185-5p, miR-221-3p, miR-21-5p, miR-210-3p), 6 texture parameters (Mean, Standard Deviation, Entropy, Mean of Positive Pixels, Skewness, Kurtosis) in 5 different spatial scaling factors (SSF0, SSF1, SSF1.5, SSF1.8, SSF2.0). All data were elaborated for normal kidney parenchyma and for 3 different ROIs on tumour volume, finally producing a total of more than 170 graphics of correlation.

Normality of each continuous variable was tested with Z-test.

Differences between normal tissue and tumour in all miRNA expression and all CTTA parameters was assessed using paired t-Student test.

First step of statistical analysis was aimed to assess statistically significant differences between the 2 groups of lesions' samples: formalin fixed (FFPE) and fresh frozen (FF).

Differences in the evaluations of CTTA parameters between the 2 operators were calculated (inter-observer agreement with Cohen's Kappa, with $k \leq 0.40$ poor agreement, $k = 0.40 – 0.75$ good agreement, $k \geq 0.76$ excellent agreement).

Secondary all lesions were evaluated all together, since no statistically significant difference in miRNA expression was found between the 2 groups and between the 2 operators for CTTA.

In addition, statistically significant difference was assessed for: (i) miRNA normal tissue vs tumour samples; (ii) CTTA parameters in normal tissue vs tumour samples.

For comparison of miRNA vs CTTA parameters was then used Pearson correlation coefficient (r): r was interpreted as follows: a negative value or less than 0.20 indicated poor agreement; a value of 0.21-0.40, fair agreement; a value of 0.41-0.60, moderate agreement; a value of 0.61-0.80, substantial agreement; and a value of 0.81-1.00, almost perfect agreement.

For all comparisons, statistical significance was assumed to be $p < 0.05$. All statistical analyses were performed by using a commercially-available statistical software package SPSS version 21.0 (SPSSInc®, Chicago, MO).

Results

Mean tumours' maximum diameter was 4.2 cm (± 2,38), with a prevalence of grading score G2 (15/20) pT1a and pT1b (16/20) at histology evaluation (Table 1).

A total of twenty matched ccRCC and adjacent normal tissue samples were collected and analysed for miRNAs expression. Interestingly, miR-21-5p, miR-210-3p and miR-221-3p resulted significantly up-regulated in ccRCC vs normal tissues ($p < 0,05$).

In particular the expression of miR-21-5p, miR-210-3p and miR-221-3p resulted particularly up-regulated in tumour samples (respectively 0.94 ± 0.61, 1.57 ± 1.32 and 1.13 ± 0.74) as compared to normal tissues (respectively 0.60 ± 0.52, 1.18 ± 0.94 and 0.71 ± 0.33) with a *p* value < 0.05; although miR-185-5p did not show any statistically significant difference between tumour and normal tissues, showed a trend of expression similar to miR-21-5p and miR-221-3p ($p > 0.05$). Moreover, miR-145-5p expression resulted particularly up-regulated in few tumour samples compared to normal tissues, and down-regulated in others (9/20) however no statistically significant difference between ccRCC and normal tissues was obtained ($p > 0.05$) (Fig. 3).

No differences were found between the 2 operators in collected CTTA parameters (k=0,84). The analyses shown, were elaborated using data from the best operator-results.

When considering texture parameters alone, differences between healthy and pathological tissue within the same SSF and the same contrast phase were consistent and statistically significant for the majority of parameters (entropy, mpp, sd and mean) when a medium texture filter setting (SSF1 or SSF1.5) was used ($p<0.05$); for these parameters it has been shown a statistically significant difference between normal tissue ROIs and pathological tissues, in all contrast phases (Table 3).

Moreover, comparing different contrast phases within the same SSF no significant differences were found in each parameter in particular between medium filters (SSF 1.5 – 1.8 – 2.0). In specific entropy values arterial phase in normal tissue were 4.66±0.21 (SF1), 4,71±0,21 (SF1.5), 4,72±0,19 (SF1.8), 4,73±0,19(SF2.0); while in tumour ROI entropy was 5.67±0.41 (SF1), 5,76±0,40 (SF1.5); 5,79±0,39 (SF1.8); 5,80±0,40 (SF 2.0) respectively.

miRNA expression in normal tissue didn't correlate with any CTTA parameter (p>0.05).

On the other side a trend of positive correlation was found between some miRNA and some CTTA parameters when tumour samples were analysed (Table 4) (Figure 4). The best trends were found when delta of expression (Δ) and delta of percent (%Δ) of expression between healthy tissue and pathological tissue were used for the expression of our data.

When comparing CT texture parameters and miRNA expression we found a dispersion of data in the graphics of comparison, showing very poor agreement with mi-RNA expressivity for most of the parameters.

Interestingly entropy showed the best results: for example, in a non-linear graphic relation between %Δ of miRNA and entropy in normal tissue and tumour samples, while miR-210-3p didn't show any relation with entropy expression, miR-21-5p was found to be the most well-correlated with entropy (arteriosus phase, SF1) with a higher coefficient of determination (R^2 is the proportion of the variance in the dependent variable that is predicted by the independent variable). These results were confirmed using all SF and all post-contrast phases. Moreover, the results are better expressed using percent Delta of miRNA expression (R^2=0,06 for miR210 and R^2=0,25 for miR21-5p).

Analysing data, we recognized 4 patients with particularly over-expressed miRNA but only slight increase of entropy (as compared to normal tissue): their texture parameters were not far from the median values of the texture parameters of the other patients, but miR-21-5p expression differ a lot from the other patients. The expression of miR-21-5p in normal tissue

was, at contrary, not far from the median values of other samples. Interestingly, excluding them from the analysis, we found again that normal tissue entropy was not related with miR-21-5p (R^2= 0,17), while texture excellent relation of entropy in tumour samples with miR21-5p was found (R^2= 0,64 fig 4).

Discussion

Evaluation of a renal lesion using CT or MRI sometimes with presumption of the histotype is nowadays based on the radiologist's 2D examination of lesion morphology and enhancement, and this routinely determines subsequent patient management.

CT and MRI are the most used imaging techniques in the staging of ccRCC before treatment; however, this type of tumours is characterized by genetic, epigenetic and pathologic heterogeneity, which makes accurate diagnosis or prognosis prediction difficult.

Many efforts have been done by radiologist and experts looking for imaging biomarkers for characterization of tumours and follow-up during therapies.

CTTA allows quantification of lesion heterogeneity based on the distribution of pixel intensities within a ROI.

CTTA is a relatively new tool with a great potential, it can be of great help for the radiologist to better characterize lesions and to identify parameters of response to treatment. However, it is still soon to consider all done.

Radiogenomics refers to the correlation between cancer imaging features and gene expression: the most interesting results are obtained in onco-imaging field.

Recently, some authors have evaluated the correlation between the imaging characteristics and molecular features of malignancies. Jain et al demonstrated that the clinical features, imaging and molecular characteristics may provide information on the portion of glioblastoma without contrast enhancement [14]. Correlations between genetic mutations and CT features were observed by Karlo et Al for ccRCC carcinoma and by Rizzo et al for NSCLC [15, 16].

Comparison of CTTA and molecular or genetics aspects of tumours has been explored in colorectal cancer by De Cecco et Al who found a correlation between changes in kurtosis values and response to radio-chemotherapy in colorectal cancer [17]. and in head & neck cancer and NSCLC by Aerts et Al who constituted a prognostic radiogenomics signature of these tumours

[18]. Sacconi et Al finally recently found a correlation between EGFR and mean, SD and skewness, and between entropy and the event of death in lung adenocarcinoma [19].

MicroRNAs are a class of small, noncoding RNAs that play a key role on post-transcriptional expression of target genes, and they are recently found to be a new class of genes with tumour-suppressor and oncogenic functions [13, 14].

In the field of urological carcinoma, miRNAs are acquiring a role as biomarkers [20, 21, 22].

In particular miRNA-21-3p is the most overexpressed in renal cancer: it interacts with Ras phosphoinositide-3- kinase (PI-3K)/PTEN/AKT apoptosis pathways so it may be considered a clinical biomarker in RCC.

In a recent publication [23] some of us recently found interesting results on overexpression of miR21 and miR210 on urinary samples, and they also prove the significant reduction in concentration of them after surgery and during follow-up. This finding seems to be very interesting, opening new doors for genetic- biomarkers in ready and "easy to collect" tissue samples.

In a radiogenomics approach we decided to compare CT texture parameters and genetic profile of ccRCC, focusing on the expression of miRNAs, looking for correlation between them.

First we confirmed deregulation of specific miRNAs in our group of 20 ccRCC (miR-21-5p, miR-210-3p, miR-185-5p, miR-145-5p and miR-221-3p), according to what found previously [24]. In particular miR-21-5p and miR-210-3p are involved in ccRCC tumorigenesis and can be considered as biomarkers for clear cell carcinoma.

In parallel most of CTTA parameters showed significant differences comparing normal cortico-medullar tissue with ccRCC. CTTA has robust parameters to distinguish normal tissue from clear cell carcinoma (e.g. entropy, mean, sd). This could be of great future help for imaging characterization of renal lesion, even in terms of survival rates and clinical outcome.

The surprising result of not significant increase of skewness and kurtosis in our cohort of ccRCC, in contrast with previous studies on other solid tumours (e.g. rectal or lung adenocarcinoma), support the fact that different tumours display different radio-phenotypes and address the attention to more research in this field, with the aim of looking for a "texture signature" typical for every tumour type.

A previous study from Lubner MG et Al [25], showed a difference between normal liver tissue and different grades of liver fibrosis, in particular finding increase of mean grey level intensity and entropy, while decrease of skewness and kurtosis, in parallel with increasing fibrosis stage.

Regarding the comparison between expression of miRNA and modification of CTTA in tumour samples, a surprisingly poor positive association was found among the majority of them in ccRCC with poor statistical significance.

Interesting results were found comparing entropy and miR-21-5p expression: no relation was found with normal tissue, while tumour entropy is slightly positively correlated. The results are almost stable moving into different contrast-phases and different spatial filters, giving to the correlation more importance.

The correlation was a bit limited by data from 4 patients (20%), who had a significant up-regulation of miR-21-5p but a slight increase of entropy in lesions as compared to normal tissues. The reason why these patients showed such results in still not clear. We couldn't find a reasonable factor to explain this behaviour, since patients performed the same CT protocol and their tissue samples were either fresh frozen (for 2) or FFPE (for the others). Furthermore, they were not different neither in terms of TNM or grading, without any apparent difference in comparison with the others. The only interesting common factor was that they were among the youngest in the cohort of patients (<60 years of age), and this could have a role in the significant hyper-expression of miRNA in tumour samples. More data are needed to support this conclusion.

Nevertheless, without those 4 patients we found more significant results with very good correlation.

Texture analysis is efficient, reproducible and it can be considered complementary to 2D imaging evaluation of ccRCC on MDCT, because it maximizes the information obtained from the lesion and it has the potential to become a tool for prediction of prognosis.

Further studies with a larger cohort of patients and focusing on prognostic value of both, miRNA and CTTA, are needed.

There are some limitations to the present study, the first is the small group of patients. Moreover, we didn’t perform analysis on prognostic value of the parameters because of lacking of outcome data: this could be the focus for our next research.

The measurements were performed on pre-treatment quite large renal masses and in 2D ROIs on three different levels of the lesions to minimize the heterogeneity in MDCT scans. This choice has been made to avoid complicated volumetric measurements, supported by literature suggesting that even a single slice measurement may be enough.[26, 27].

Conclusion

In conclusion miRNA and CTTA show interesting correlations in ccRCC and no correlations with normal tissues. In particular there is a correlation between entropy and miRNA 21-5p, one of the most important miRNA involved in tumorigenesis; in addiction our results reveal that CT texture features, in particular mean and entropy, are correlated with ccRCC. This type of information can be considered a useful non-invasive adjunct to biopsy results in prognostication and patient management.

Fig. 1

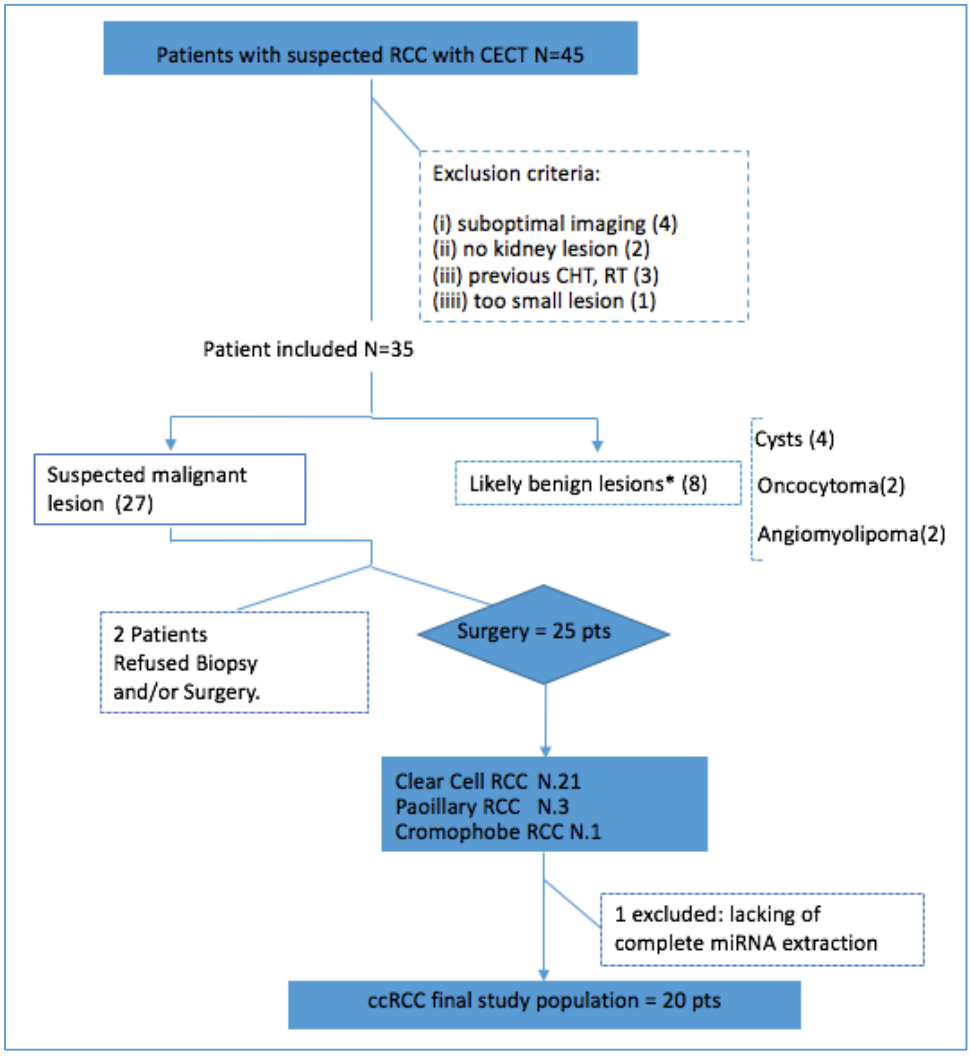

Fig. 1 Flowchart of patients

Tab. 1

Patient demographics and characteristics at diagnosis	
Number of patients	20
Age (years)	65±3
Gender	
Male Female	14 6
Body Mass Index	
	27 kg/m2 ± 4,37
Serum Creatinine	
	1,45 ± 0,72 (mg/dl)
Smoking habit	
yes no	13 7
Patological Tumour stage (pT)	
pT1a	11
pT1b	4
pT2a	1
pT2b	1
pT3	3
Surgical procedure	
Tumorectomy Radical nefrectomy	7 13
Clear cell tumour grade	
1 2 3	3 15 2
Tomour Maximum Diameter	
	4,2± 2,4 cm
Abbreviations: MSKCC= Memorial Sloan-Kettering Cancer Centre; OS=overall survival; PFS=progression-free survival	

Tab. 1 Patient clinical and histological characteristics

Table 2

MDCT parameters	
Detector Configuration [mm]	64 x 0.625
Tube Voltage [kV]	120
Automatic exposure control (AEC)	On
Current tube modulation [mAs]	200/600
Noise index	28
Field of View [cm]	50
Rotation Time [sec.]	0.5
Pitch	1.375
Reconstruction Kernel	Medium-Smooth
Reconstruction Algorithm	Q30
Iterative reconstruction algorithm	40%
Slice thickness [mm]	1.25

Table 2. CT acquisition and reconstruction parameters**.**

Table 3

Arterial Phase SSF 1.5	*Normal tissue*	*Tumour*	*p- value*	*p-value Venous Phase*	*p value Urographic phase*
mean	-1.23 (±14.7)	23.31 (± 17.38)	<0.001	<0.05	<0.05
sd	101,2 (±37.8)	120.9 (±32.7)	<0.05	0.09	0.06
entropy	4.71 (±0.20)	5.76 (±0.40)	<0.001	<0.05	<0.05
mpp	85.39 (±38.75)	107.17 (±33.1)	<0.05	<0.05	<0.05
skewness	0.25 (±0.42)	0.36 (±0.49)	0.45	0.52	0.30
kurtosis	-0,04 (±0.63)	1.67 (±5.50	0.17	0.23	0.10

Table 3. expression of CTTA texture parameters in normal tissue and tumour in arterial phase. *p* – values are shown for arterious, venous and urographyc phase.

Figure 2

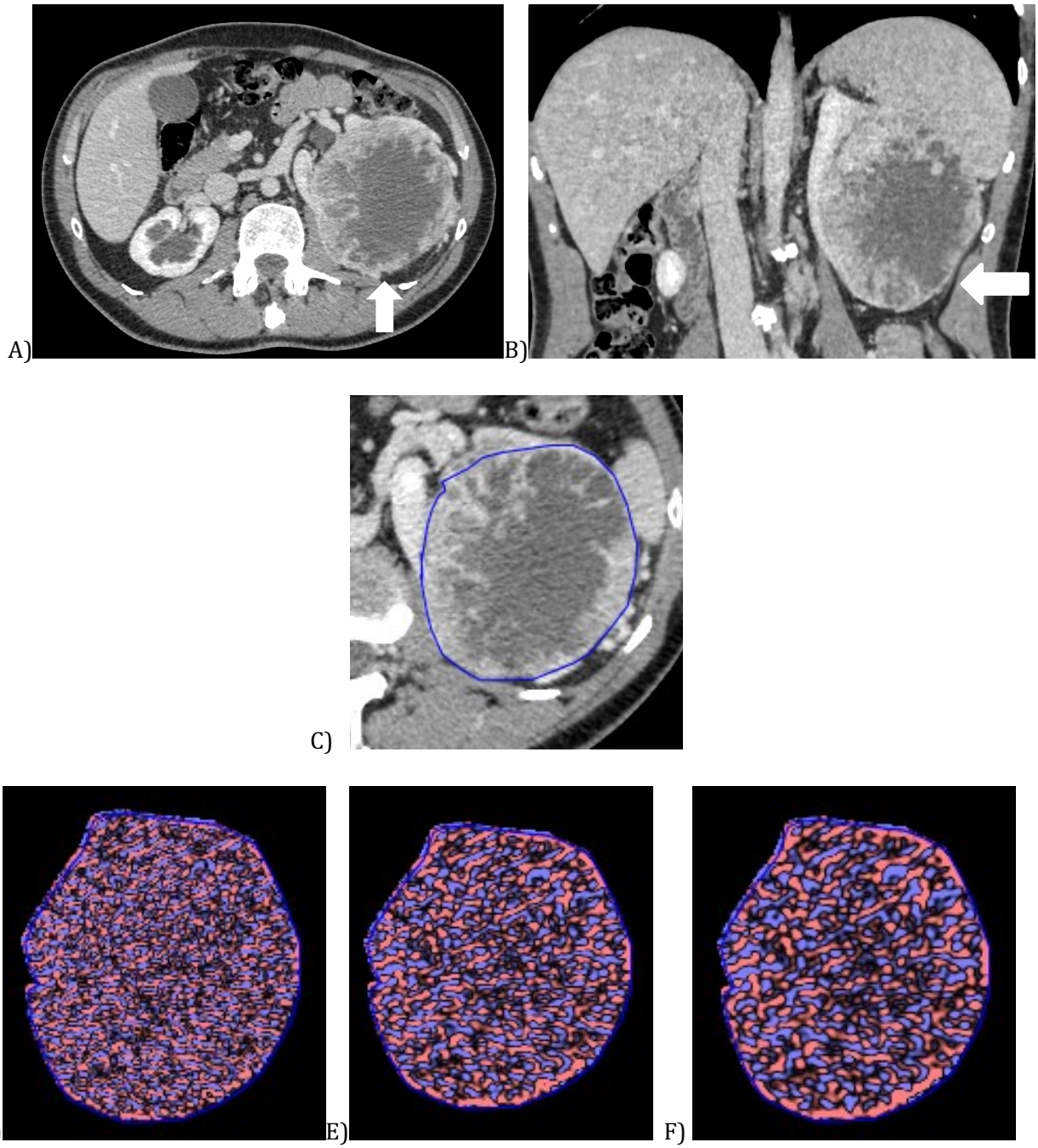

Figure 2.- 58 years old man with a large ccRCC on left side.
A)- B). Portal venous phase contrast enhanced transverse (A) and coronal (B) CT images show tumour (arrows). C). Texture analysis image show ROI (blue line) outlining cancer. D)-F). Colour texture overlays of cancer outlined by a ROI (blue line) show images with a fine filtering (spatial scaling factor, 1) (D), medium filtering (spatial scaling factor, 1.5) (E), and coarse filtering (spatial scaling factor, 2) (F).

Figure 3

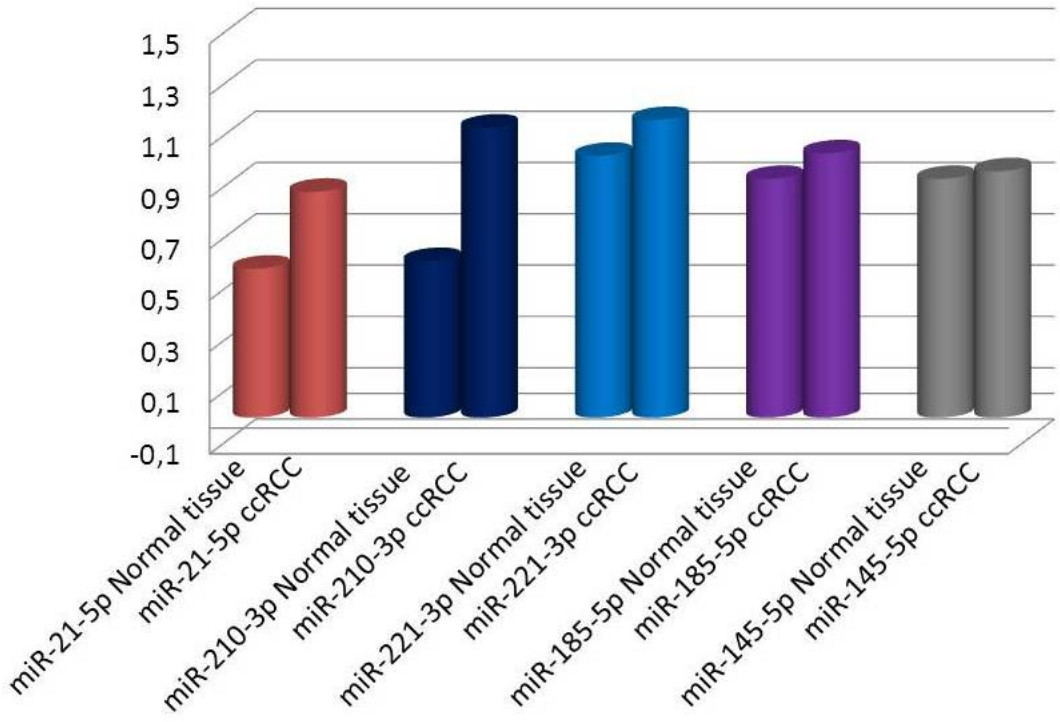

	Mean values microRNAs levels (± SD)				
	miR-21-5p	**miR-210-5p**	**miR-221-3p**	**miR-185-5p**	**miR-145-5p**
Normal tissue	0.60 (± 0.51)	1.18 (± 0.94)	0.71 (± 0.32)	1.08 (± 0.96)	1.04 (± 0.33)
ccRCC	0.94 (± 0.61)	1.57 (± 1.31)	1.13 (± 0.74)	1.03 (± 0.47)	1.14 (± 0.65)
***p* value**	< 0.05	< 0.05	< 0.05	> 0.05	> 0.05

Figure 3. Evaluation of microRNAs levels in clear cell renal cell carcinoma (ccRCC) patients

Tab. 4

normal tissue	mean	SD	entropy	mpp	skewness	kurtosis
Δ (%) miR-21	0.30	-0.14	0.06	-0.10	-0.21	0.09
Δ (%) miR 210	-0.09	-0.26	0.23	-0.27	-0.28	-0.21
tumour	**mean**	**SD**	**entropy**	**mpp**	**skewness**	**kurtosis**
Δ (%) miR-21	-0.24	0.07	0.24	0.007	0.04	0.09
Δ (%) miR 210	0.11	0.15	0.09	0.17	-0.01	-0.13

Tab. 4 CTTA parameters and miRNA Pearson correlation coefficient *r*. Statistically significant results are signed with *

Figure 4

A)

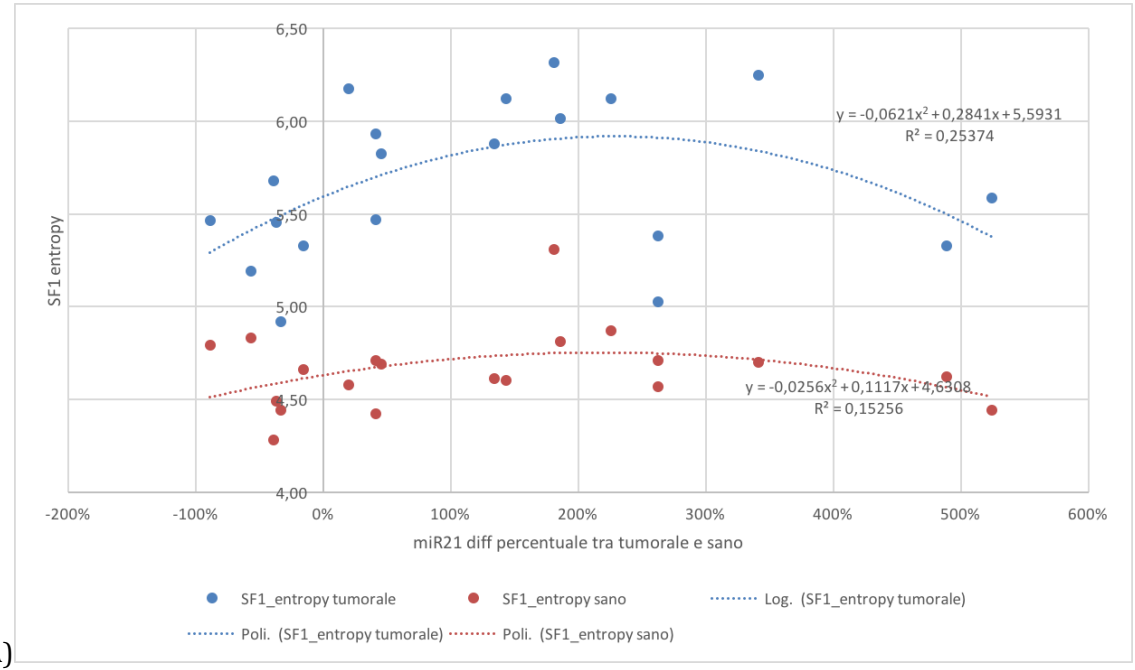
6,50
6,00
5,50
5,00
4,50
4,00
SF1 entropy
y = -0,0621x² + 0,2841x + 5,5931
R² = 0,25374
y = -0,0256x² + 0,1117x + 4,6308
R² = 0,15256
-200%
-100%
0%
100%
200%
300%
400%
500%
600%
miR21 diff percentuale tra tumorale e sano
SF1_entropy tumorale
SF1_entropy sano
Log. (SF1_entropy tumorale)
Poli. (SF1_entropy tumorale)
Poli. (SF1_entropy sano)

B)

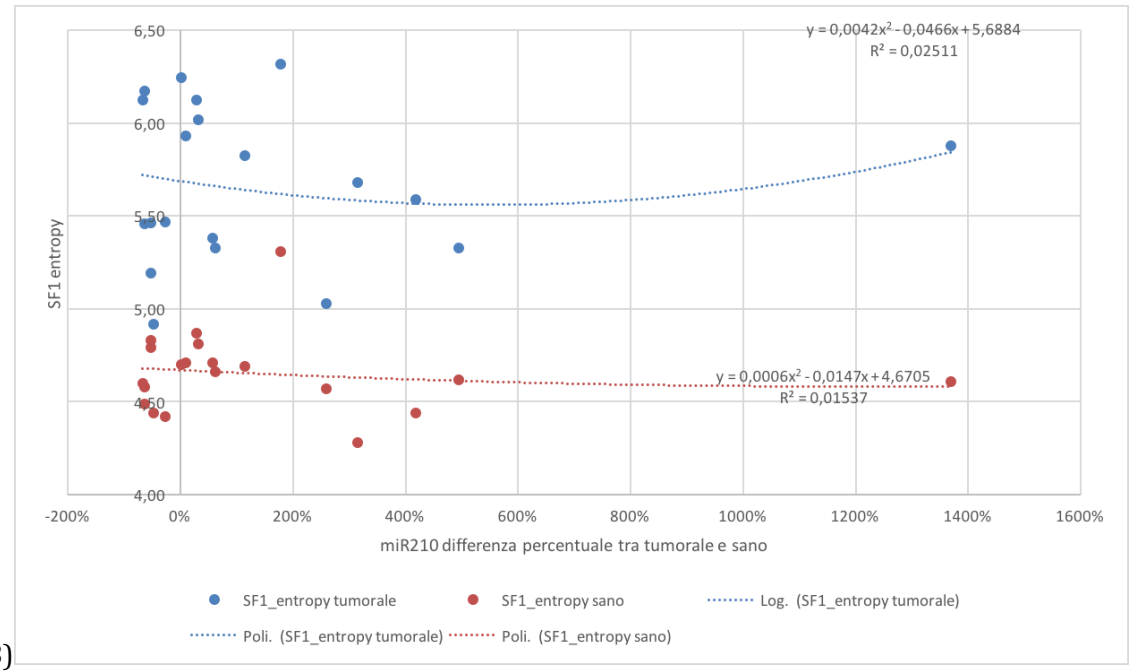
6,50
6,00
5,50
5,00
4,50
4,00
SF1 entropy
y = 0,0042x² - 0,0466x + 5,6884
R² = 0,02511
y = 0,0006x² - 0,0147x + 4,6705
R² = 0,01537
-200%
0%
200%
400%
600%
800%
1000%
1200%
1400%
1600%
miR210 differenza percentuale tra tumorale e sano
SF1_entropy tumorale
SF1_entropy sano
Log. (SF1_entropy tumorale)
Poli. (SF1_entropy tumorale)
Poli. (SF1_entropy sano)

C)

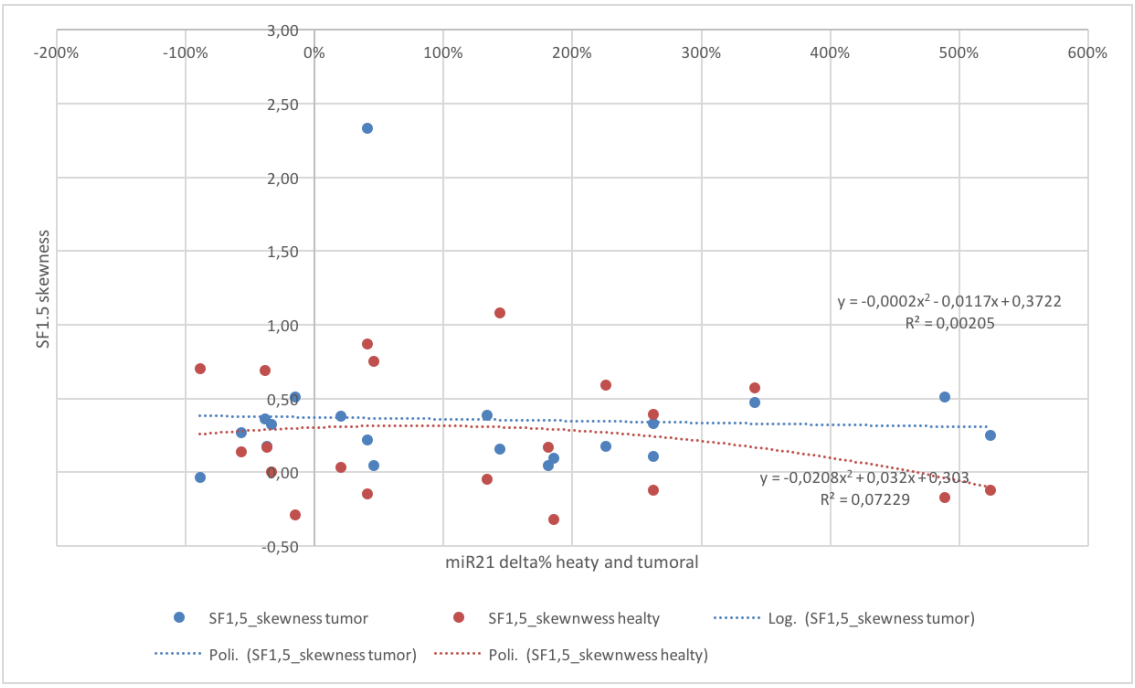

Fig. 4. graphics of relation and R^2 value between microRNAs and CTTA features in ccRCC. A) On the x-axis are shown %Δ of mir-21-3p, on the y axis are shown separately, normal tissue entropy and tumour tissue entropy (SSF1). B) x axis: %Δ miR 210-3p; y axis normal tissue entropy and tumour tissue entropy (SSF1) C) x axis: %Δ miR 21-3p; y axis normal tissue skewness and tumour tissue skewness (SSF1.5)

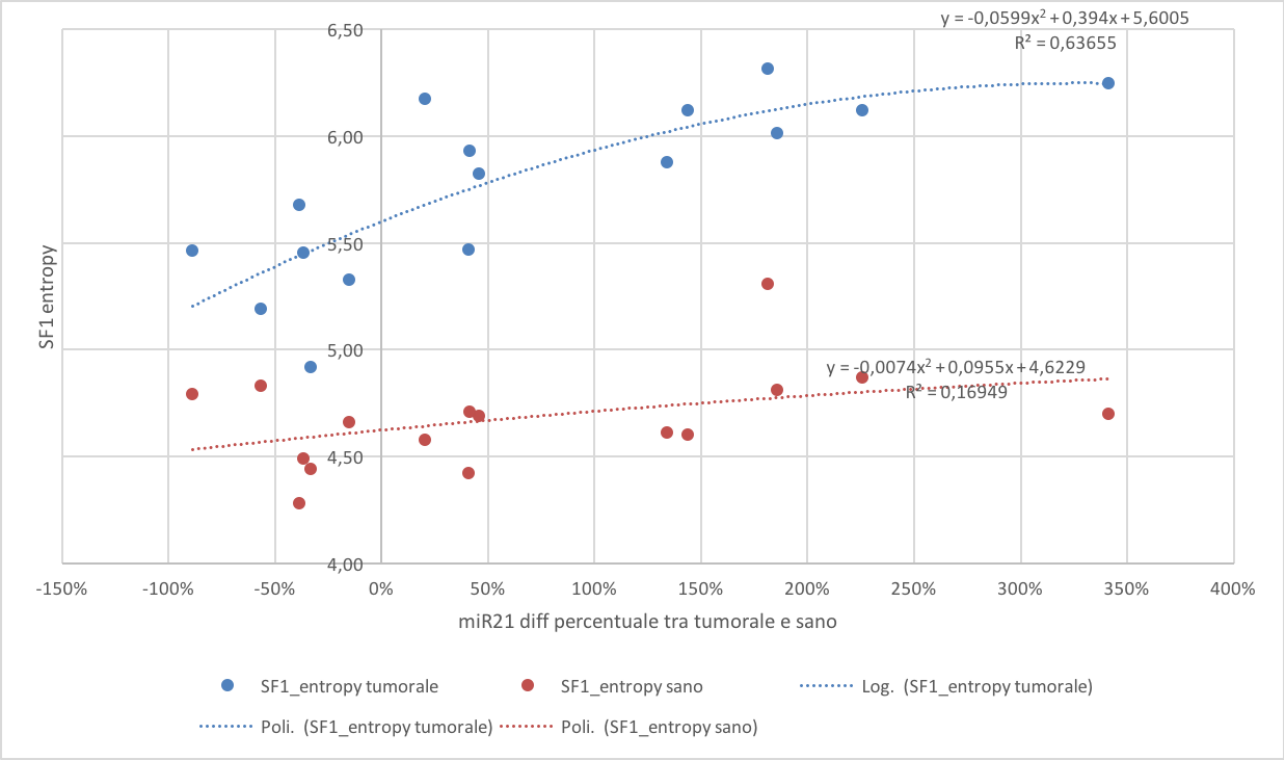

Fig. 5 Graphic of comparison between miR-21 (expressed as %Δ normal vs tumour) and entropy excluding 4 patients with extremely over-expression of miR-21 in tumour samples (too far from median values). As shown normal tissue entropy have a worst relation than tumour tissue with miR21-3p. This latter relation is very good with a R^2 of 0.64

Bibliography

1. Siegel R, Naishadham D, Jemal A: Cancer statistics, 2013. *CA Cancer J Clin* 2013, 63(1):11-30.

2. Jonasch E, Futreal PA, Davis IJ, Bailey ST, Kim WY, Brugarolas J, Giaccia AJ, Kurban G, Pause A, Frydman J *et al*: State of the science: an update on renal cell carcinoma. *Molecular cancer research : MCR* 2012, 10(7):859-880.

3. Schaefer A, Stephan C, Busch J, Yousef GM, Jung K: Diagnostic, prognostic and therapeutic implications of microRNAs in urologic tumors. *Nature reviews Urology* 2010, 7(5):286-297.

4. Fridman E, Dotan Z, Barshack I, David MB, Dov A, Tabak S, Zion O, Benjamin S, Benjamin H, Kuker H *et al*: Accurate molecular classification of renal tumors using microRNA expression. *The Journal of molecular diagnostics : JMD* 2010, 12(5):687-696.

5. Cowland JB, Hother C, Gronbaek K: MicroRNAs and cancer. *APMIS : acta pathologica, microbiologica, et immunologica Scandinavica* 2007, 115(10):1090-1106.

6. Shuch B, Bratslavsky G, Linehan WM, Srinivasan R: Sarcomatoid renal cell carcinoma: a comprehensive review of the biology and current treatment strategies. *The oncologist* 2012, 17(1):46-54.

7- Cancer Genome Atlas Research Network. Comprehensive molecular characterization of clear cell renal cell carcinoma. Nature 2013, 499, 43–49

8 Osanto, S.; Qin, Y.; Buermans, H.P.; Berkers, J.; Lerut, E.; Goeman, J.J.; van Poppel, H. Genome-wide microRNA expression analysis of clear cell renal cell carcinoma by next generation deep sequencing. PLoS ONE 2012, 7, e38298.

9 Gowrishankar, B.; Ibragimova, I.; Zhou, Y.; Slifker, M.J.; Devarajan, K.; Al-Saleem, T.; Uzzo, R.G.; Cairns, P. MicroRNA expression signatures of stage, grade, and progression in clear cell RCC. Cancer Biol. Ther. 2014, 15, 329–341

10 Ge, Y.Z.;Wu, R.; Xin, H.; Zhu, M.; Lu, T.Z.; Liu, H.; Xu, Z.; Yu, P.; Zhao, Y.C.; Li, M.H.; et al. A tumor-specific microRNA signature predicts survival in clear cell renal cell carcinoma. J. Cancer Res. Clin. Oncol. 2015, 141, 1291–1299

11 Tang, K.; Xu, H. Prognostic value of meta-signature miRNAs in renal cell carcinoma: An integrated miRNA expression profiling analysis. Sci. Rep. 2015, 5.

12 Lu, G.J.; Dong, Y.Q.; Zhang, Q.M.; Di, W.Y.; Jiao, L.Y.; Gao, Q.Z.; Zhang, C.G. miRNA-221 promotes proliferation, migration and invasion by targeting TIMP2 in renal cell carcinoma. Int. J. Clin. Exp. Pathol. 2015, 8, 5224–5229

13. Al-Kadi OS, Watson D: Texture analysis of aggressive and nonaggressive lung tumor CE CT images. *IEEE transactions on bio-medical engineering* 2008, 55(7):1822-1830.

14. Jain R, Poisson LM, Gutman D, Scarpace L, Hwang SN, Holder CA, Wintermark M, Rao A, Colen RR, Kirby J *et al*: Outcome prediction in patients with glioblastoma by using imaging, clinical, and genomic biomarkers: focus on the nonenhancing component of the tumor. *Radiology* 2014, 272(2):484-493.

15. Karlo CA, Di Paolo PL, Chaim J, Hakimi AA, Ostrovnaya I, Russo P, Hricak H, Motzer R, Hsieh JJ, Akin O: Radiogenomics of clear cell renal cell carcinoma: associations between CT imaging features and mutations. *Radiology* 2014, 270(2):464-471.

16. Rizzo S, Petrella F, Buscarino V, De Maria F, Raimondi S, Barberis M, Fumagalli C, Spitaleri G, Rampinelli C, De Marinis F *et al*: CT Radiogenomic Characterization of EGFR, K-RAS, and ALK Mutations in Non-Small Cell Lung Cancer. *European radiology* 2016, 26(1):32-42.

17. De Cecco CN, Ganeshan B, Ciolina M, Rengo M, Meinel FG, Musio D, De Felice F, Raffetto N, Tombolini V, Laghi A: Texture analysis as imaging biomarker of tumoral response to neoadjuvant chemoradiotherapy in rectal cancer patients studied with 3-T magnetic resonance. *Investigative radiology* 2015, 50(4):239-245.

18. Aerts HJ, Velazquez ER, Leijenaar RT, Parmar C, Grossmann P, Carvalho S, Bussink J, Monshouwer R, Haibe-Kains B, Rietveld D *et al*: Decoding tumour phenotype by noninvasive imaging using a quantitative radiomics approach. *Nature communications* 2014, 5:4006.

19 Sacconi B, Anzidei M, Leonardi A et al: Analysis of CT features and quantitative texture analysis in patients with lung adenocarcinoma: a correlation with EGFR mutations and survival rates *Clinical Radiology* 2017, 72(6):443-450.

20 Fendler A, Stephan C, Yousef GM, Kristiansen G, Jung K. The translational potential of microRNAs as biofluid markers of urological tumours. Nature reviews Urology. 2016; 13: 734-752.

21 Lou N, Ruan AM, Qiu B, Bao L, Xu YC, Zhao Y, Sun RL, Zhang ST, Xu GH, Ruan HL, Yuan CF, Han WW, Shi HC, Yang HM, Zhang XP. miR-144-3p as a novel plasma diagnostic biomarker for clear cell renal cell carcinoma. Urologic oncology. 2017; 35: 36 e37-36 e14

22 Mlcochova H, Hezova R, Stanik M, Slaby O. Urine microRNAs as potential noninvasive biomarkers in urologic cancers. Urologic oncology. 2014; 32: 41 e41-49

23 Petrozza V, Pastore AL, Palleschi G *et al*: Secreted miR-210-3p as non invasive biomarker in clear cell renal cell carcinoma, Oncotarget, Advance Pubblication 2017; www.impactjournals.com/oncotarget

24. Petrozza V, Carbone A, Bellissimo T, Porta N, Palleschi G, Pastore AL, Di Carlo A, Della Rocca C, Fazi F: Oncogenic MicroRNAs Characterization in Clear Cell Renal Cell Carcinoma. *International journal of molecular sciences* 2015, 16(12):29219-29225.

15. Lubner MG, Stabo N, Abel EJ, Del Rio AM, Pickhardt PJ: CT Textural Analysis of Large Primary Renal Cell Carcinomas: Pretreatment Tumor Heterogeneity Correlates With Histologic Findings and Clinical Outcomes. *AJR American journal of roentgenology* 2016, 207(1):96-105.

16. Lubner MG, Stabo N, Lubner SJ, del Rio AM, Song C, Halberg RB, Pickhardt PJ: CT textural analysis of hepatic metastatic colorectal cancer: pre-treatment tumor heterogeneity correlates with pathology and clinical outcomes. *Abdominal imaging* 2015, 40(7):2331-2337.

17. Ng F, Kozarski R, Ganeshan B, Goh V: Assessment of tumor heterogeneity by CT texture analysis: can the largest cross-sectional area be used as an alternative to whole tumor analysis? *European journal of radiology* 2013, 82(2):342-348.